ORIGINAL RESEARCH

Dysfunction of Myosin Light-Chain 4 (MYL4) Leads to Heritable Atrial Cardiomyopathy With Electrical, Contractile, and Structural Components: Evidence From Genetically-Engineered Rats

Wenhui Peng, MD, PhD;* Miaoxin Li, PhD;* Hailing Li, MD, PhD;* Kai Tang, MD, PhD; Jianhui Zhuang, MD, PhD; Jianguo Zhang, PhD; Jingjing Xiao, PhD; Hui Jiang, PhD; Dali Li, PhD; Yongchun Yu, PhD; Pak C. Sham, PhD; Stanley Nattel, MD; Yawei Xu, MD, PhD

***Background*—**There is increasing interest in the concept of atrial cardiomyopathy, but the underlying molecular and mechanistic determinants remain poorly defined. We identified a family with heritable atrial cardiomyopathy manifesting as progressive atrial-selective electromechanical dysfunction, tachyarrhythmias, and bradyarrhythmias requiring pacemaker implantation. Myosin light-chain 4 (*MYL4*), encoding the atrial-selective essential myosin light chain, was identified as a candidate gene. We used genetically modified rat models to investigate the role of *MYL4* in atrial cardiomyopathy.

***Methods and Results*—**Exome sequencing and systematic bioinformatic analyses identified a rare missense variant of *MYL4* (c.31G>A [*p.E11K*]) in a large multiplex atrial cardiomyopathy family pedigree. The mutation cosegregated with atrial standstill (selected as the principal presenting trait) with a logarithm of the odds score of 5.3. The phenotype of rats with *MYL4* mutation knock-in confirmed the causative role of the mutation. *MYL4* knockout rats showed a similar atrial cardiomyopathy phenotype, whereas rats with an adjacent 4-amino-acid deletion showed no phenotype. Both *MYL4 p.E11K* knock-in rats and *MYL4* knockout rats showed progressive atrial electrophysiological, contractile, and fibrotic abnormalities, similar to affected patients. Biochemical analyses of *MYL4 p.E11K* mutation rats showed activation of proapoptotic and profibrotic signaling, along with increased atrial-cardiomyocyte terminal deoxynucleotidyl transferase dUTP nick end labeling staining, suggesting enhanced apoptotic cell death, findings that were mimicked by in vitro adenoviral transfer of the mutant gene to neonatal-rat cardiomyocytes.

***Conclusions*—**Loss-of-function *MYL4* gene variants cause progressive atrial cardiomyopathy in humans and rats. Our findings identify *MYL4* as a key gene required for atrial contractile, electrical and structural integrity. These results improve our understanding of the molecular basis of atrial cardiomyopathy and introduce new models for further mechanistic analysis. **(*J Am Heart Assoc*. 2017;6:e007030. DOI; 10.1161/JAHA.117.007030.)**

Key Words: animal models • arrhythmia • atrial fibrillation • cardiomyopathy • fibrosis • genetics

Whereas ventricular cardiomyopathy is a well-established entity with clear diagnostic and therapeutic implications, atrial cardiomyopathy represents a relatively new concept in active development.[1] A wide range of factors contributes to the development of atrial cardiomyopathy, most commonly in association with ventricular pathology.[1] To

From the Department of Cardiology, Shanghai Tenth People's Hospital, School of Medicine, Tongji University, Shanghai, China (W.P., H.L., K.T., J. Zhuang, Y.X.); Department of Psychiatry, Centre for Genomic Sciences (M.L., P.C.S.) and State Key Laboratory for Brain and Cognitive Sciences (M.L., P.C.S.), The University of Hong Kong, Pokfulam, Hong Kong; Department of Medicine, Montreal Heart Institute, Montreal, Quebec, Canada (S.N.); Université de Montréal, Quebec, Canada (S.N.); Department of Pharmacology and Therapeutics, McGill University, Montreal, Quebec, Canada (S.N.); Institute of Pharmacology, West German Heart and Vascular Center, University Duisburg-Essen, Essen, Germany (S.N.); Department of Medical Genetics, Center for Genome Research, Center for Precision Medicine, Zhongshan School of Medicine, Sun Yat-sen University, Guangzhou, China (M.L.); Shanghai Traditional Chinese Medicine Hospital, Shanghai University of Traditional Chinese Medicine, Shanghai, China (Y.Y.); Shanghai Key Laboratory of Regulatory Biology, Institute of Biomedical Sciences and School of Life Sciences, East China Normal University, Shanghai, China (D.L.); BGI-Shenzhen, Shenzhen, China (J. Zhang, J.X., J.H.).

Accompanying Data S1, Tables S1 through S12, and Figures S1 through S10 are available at http://jaha.ahajournals.org/content/6/11/e007030/DC1/embed/inline-supplementary-material-1.pdf

*Dr Peng, Dr Miaoxin Li, and Dr Hailing Li are co-first authors.

Correspondence to: Yawei Xu, MD, PhD, Department of Cardiology, Shanghai Tenth People's Hospital, Tongji University School of Medicine, 301 Middle Yanchang Rd, Shanghai 200072, China. E-mail: xuyawei@tongji.edu.cn

Received July 27, 2017; accepted August 30, 2017.

Clinical Perspective

What Is New?

- Here, we study a kindred with several members showing a severe atrial cardiomyopathy phenotype and identify a myosin light-chain 4 (*MYL4*) loss-of-function mutation as the probable cause.
- Rat models, created by knocking out the *MYL4* gene as well as by knocking in the human *MYL4 p.E11K* mutation, reproduce the clinical phenotype and point to enhanced apoptotic and profibrotic signaling as a central mechanism, providing new insights into the molecular basis of atrial cardiomyopathy.

What Are the Clinical Implications?

- MYL4 is essential for atrial electrical, functional, and structural integrity, and MYL4 dysfunction can produce severe inherited atrial cardiomyopathy.

date, few primary cardiomyopathies with highly atrial-selective manifestations have been recognized, but these may be very instructive about the mechanisms underlying the broad range of atrial cardiomyopathies.[2] Genetic analyses of atrial cardiomyopathy are, so far, limited.[2] Mutations in the natriuretic peptide precursor A gene are associated with familial atrial cardiomyopathy; long-term follow-up of natriuretic peptide precursor A–mutant patients shows progressive fibrosis associated with atrial standstill, a severe clinical scenario characterized by complete loss of atrial excitability.[3]

Myosin light-chain 4 (*MYL4*) encodes an essential myosin light chain that is specifically expressed in human atria after birth.[4] The essential light chain forms part of the actomyosin cross-bridge, providing structural support for the α-helical neck region of the myosin heavy chain and modulating actin-activated ATPase activity.[5] The ventricular analog, a protein encoded by *MYL3*, is downregulated in failing or hypertrophied hearts and partly replaced by re-expression of *MYL4* in the context of the fetal-pattern remodeling typical of ventricular pathology.[4] Recently, Gudbjartsson et al reported that *MYL4* is linked to atrial cardiomyopathy,[6,7] with a frameshift mutation in *MYL4* associated with early-onset familial atrial fibrillation (AF) and bradyarrhythmias requiring pacemaker insertion. Orr et al[8] also reported that heterozygous *MYL4 p.Glu11Lys* mutation causes familial AF. They found that expression of the analogous mutation in zebrafish leads to atrial enlargement and electrical abnormalities, without AF per se. This work presents the only animal-model data available regarding the pathophysiology associated with MYL4-dysfunction, and is limited by the fact that the zebrafish has a primitive heart tube with only 1 atrial and ventricular chamber, with (unlike humans) equal atrial and ventricular expression of the orthologous gene.

We identified a Chinese family with atrial tachyarrhythmias, a high incidence of atrial standstill, and severe bradyarrhythmias. Based on exome sequencing of this family, we identified a rare missense variant of *MYL4* (*p.E11K*), which had perfect cosegregation with atrial standstill in a large multiplex pedigree. Because these studies suggested that the MYL4 was crucial for atrial functional integrity, we generated a series of rat models using CRISPR/Cas9-mediated genome editing to define the function of MYL4, as well as to validate the ability of MYL4 dysfunction to cause the atrial abnormalities we found in patients and to define underlying mechanisms.

Methods

Additional methodological details are available in Data S1.

Large Atrial Standstill Pedigree and Clinical Features

We collected a large pedigree in which 6 family members were diagnosed as showing atrial standstill. The inheritance pattern was very likely to be autosomal dominant (Figure 1A). The proband and her family members provided written informed consent for the study according to a clinical research protocol approved by the Ethics Committee of Shanghai Tenth People's Hospital.

Standard 12-lead ECG and transthoracic echocardiography (TTE) were used to analyze atrial electrical and mechanical activity, respectively. TTE parameters of the affected patients are shown in Table S1. The diagnosis of atrial standstill was established according to the following criteria: absence of P wave on the surface 12-lead ECG; inability to stimulate the atria on invasive electrophysiological study[9]; and/or loss of the A wave on TTE. Examples of illustrative ECG and TTE data are shown in Figure 1B and 1C.

Exome Sequencing

DNA were extracted from peripheral blood. After excluding mutations in *SCN5A* and *GJA5* known to cause atrial standstill by Sanger sequencing, we performed high-throughput exome capture sequencing for 2 affected family members, II1 and II3, at the Beijing Genomics Institute in Shenzhen China (for details, see Data S1).

Calling and Prioritizing Exome Sequence Variants

The paired-end short reads from exome sequencing were mapped onto the UCSC human reference genome by BWA.[10] The Genome analysis toolkit (GATK)[11] was used to recalibrate

the alignments and to call single-nucleotide variants and short insertion-deletions (Indels). We prioritized the sequence variants by multilayer resources and functions using KGGSeq (V0.8), (http://grass.cgs.hku.hk/limx/kggseq/).[12] For details, see Data S1.

Validation of Candidate Mutations and Genes

A short list of sequence variants prioritized by KGGSeq (V0.8) was validated for all available family members by Sanger sequencing. In addition, for validated sequence variants showing perfect cosegregation with disease, we examined the frequency of mutant alleles in 200 unrelated controls without history of heart disease by Sanger sequencing. In the genomic region perfectly cosegregating with disease, we genotyped 47 sequence variants (covering around 38 Mbp) in all family members by Sequenom MassARRAY system (Sequenom, San Diego, CA). SimWalk2 was used to calculate the logarithm of the odds scores of multipoint parametric linkage analysis.[13] We then ranked all genes in the significant linkage region according to their pathogenic potential with 2 widely used bioinformatics tools, Endeavour[14] and GeneWanderer.[15] Based on this information and the literature, we identified an *MYL4* point mutation (31 G→A), causing a glutamic acid to lysine mutation at position 11, as the most likely causative candidate.

Generation of *MYL4 p.E11K* Rats, *MYL4 KO* Rats, and *MYL4 Deletion* Rat Models

All the animal procedures conformed to NIH guidelines (Guide for the Care and Use of Laboratory Animals) and were approved by the Animal Care and Use Committees of Shanghai Tenth People's Hospital.

MYL4 mutant rat strains were generated by CRISPR/Cas-mediated genome editing. In brief, Cas9 mRNA and sgRNA targeting exon 1 of *MYL4* gene was in vitro synthesized as previously described.[16,17] One-cell rat embryos were obtained by superovulation of females the next morning after mating. The zygotes were cultured in KSOM embryo culture medium (Millipore, Billerica, MA) before injection. TE solution containing 12.5 ng/μL of gRNA and ≈25 ng/μL of Cas9 mRNA was injected into the cytoplasm of 1-cell embryos through the microinjection needle. Injections were performed using an Eppendorf transferMan NK2 micromanipulator. Injected embryos were transferred into pseudopregnant female rats immediately after injection. Tail genomic DNA of F0 rats was extracted and amplified for sequencing.

Surface ECG and TTE

Surface ECGs were recorded with a biological signal acquisition amplifier (BL-420S; Taimeng Co, Chengdu, China). For TTE, transthoracic 2-dimensional and M-mode images were obtained with a Visualsonics high resolution VEVO 2100 system (VisualSonics, Toronto, Ontario, Canada) with a 20-MHz transducer. For details, see Data S1.

Immunohistochemistry

Serial 5-mm-thick atrial cryosections were stained with Masson trichrome, counterstained with hematoxylin, and quantified with Image-Pro Plus 6.0 software (version 6.0; Media Cybernetics, Inc, Rockville, MD). Fibrosis was quantified and expressed as percent cross-sectional area, excluding blood vessels and perivascular tissue. Terminal deoxynucleotidyl transferase dUTP nick end labeling staining (Roche 11684817910 kit; F. Hoffmann-La Roche AG, Basel, Switzerland) was used as an index of apoptosis. Fluorescence images were obtained with a DMI6000 fluorescent microscope (Leica Microsystems Wetzlar GmbH, Wetzlar, Germany). The sources of the primary antibodies are listed in Table S2.

Statistical Analysis

Continuous variables were described as mean±SEM. Normal distribution was verified with the Shapiro–Wilk test. If data were normally distributed, differences were analyzed by 1-way ANOVA, following by post hoc analysis (*t* test with Bonferroni correction) to evaluate statistical significance. For data that were not normally distributed, a nonparametric multiple-group comparison (Kruskal–Wallis) was performed, followed by a Wilcoxon test with Bonferroni post hoc correction to compare individual group means. All *P* values are 2-sided. The null hypothesis was rejected at $P<0.05$.

Results

Clinical Profile

We collected an unusually large pedigree of a family with inherited atrial cardiomyopathy and atrial standstill as a prominent feature, affecting 6 individuals of 44 family members distributed into 2 branches, with a typical dominant inheritance pattern (Figure 1A). The proband (I-7) initially visited our hospital for bradycardia (Figure 1B, left) and lower extremity edema. Atrial flutter with a slow ventricular response was followed approximately 4 years later by atrial standstill, neither right nor left atria could be captured during invasive electrophysiological (Figure S1A). II-1 and II-3 also developed total atrial standstill (Figure 1B, right): Although they were implanted with dual chamber pacemakers, their atria could not be captured by atrial pacing. These patients had very similar clinical histories, all suffering from bradycardia at around 20 years old, followed by palpitations and

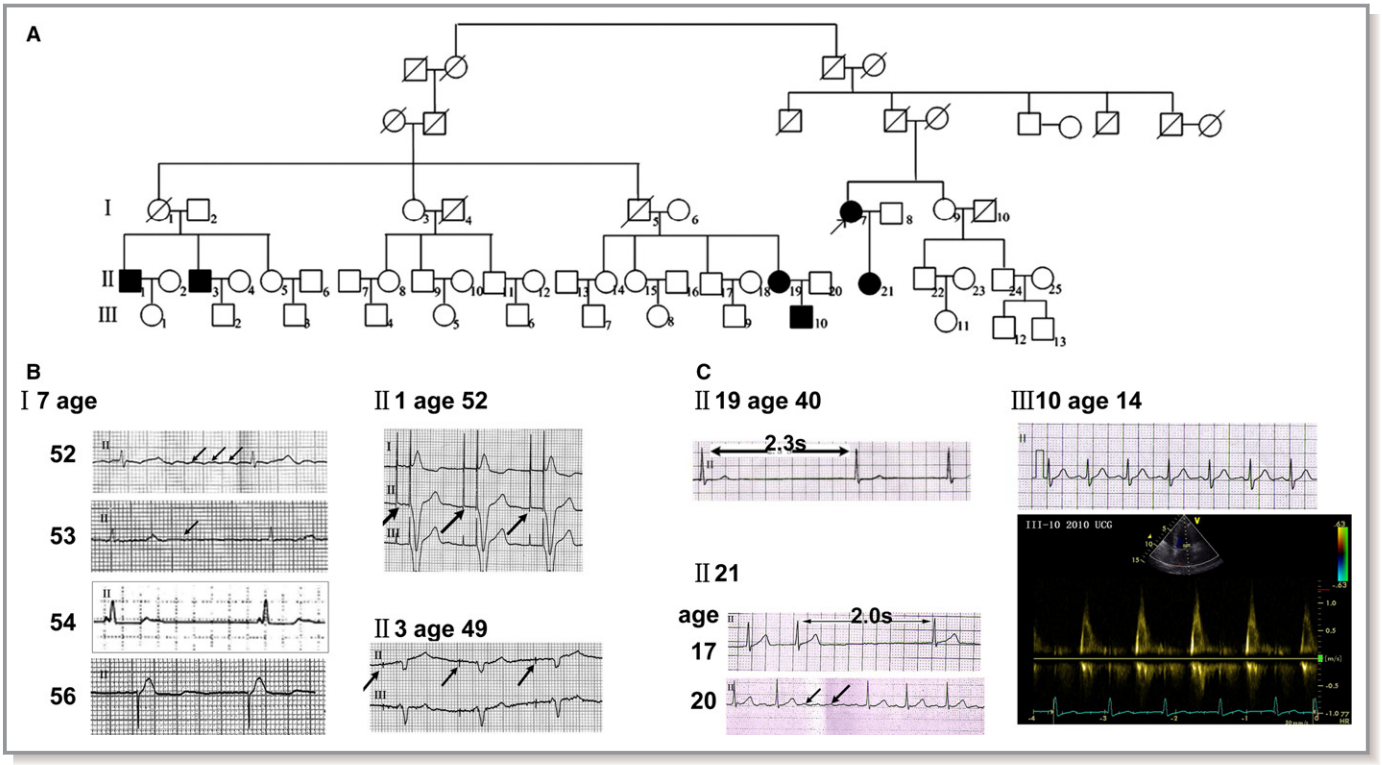

Figure 1. Pedigree and clinical data of the atrial standstill family. A, Pedigree of the atrial standstill family, 44 family members were clinically evaluated and 6 were diagnosed as having atrial standstill. B, The ECG records of the 3 patients (I-7, II-1, and II-3) with total atrial standstill: The proband (I-7) had atrial flutter (indicated by arrows) with junctional escape rhythm and atrial fibrillation at different ages and finally developed atrial standstill and required pacemaker implantation. Another 2 patients (II-1, II-3) also required pacemaker implantation; no P waves were found after atrial pacing artifacts (indicated by arrows). C, II-19, II-21, and III-10 were diagnosed as having partial atrial standstill. III-10, aged 14, had a normal ECG and no symptoms of palpitations or syncope. Though P waves were found in the surface ECGs of these patients, the A wave was absent on TTE. Atrial flutter, atrial fibrillation (II-19), and sinus arrest (pauses up to 2.3 seconds in II-19) occurred when they aged. ECG indicates standard 12-lead electrocardiography; TTE, transthoracic ultrasound.

reduced exercise tolerance between 30 and 40 years of age. After 40, all patients developed symptoms of heart failure.

II-19, II-21, and III-10 showed partial atrial standstill (Figure 1C). II-19 and II-21 had a history of paroxysmal AF with junctional escape rhythm, along with low-amplitude P waves and sinus-node dysfunction (Figure 1C and Figure S1). III-10, aged 14, had a normal ECG and no symptoms of palpitation or syncope (Figure 1C), but markedly diminished atrial contractility on TTE. Despite the P wave in the surface ECG of these patients, the A wave was markedly reduced or absent on TTE.

No atrial or ventricular septal defects or valvular abnormalities were found in these patients. Details of ECG evolution as a function of age can be found in Figure S1. Detailed ECG and TTE data are provided in Tables S1 and S3, respectively.

Novel Candidate Genes Suggested by Exome Sequencing and Bioinformatic Analysis

We then searched for candidate causal gene variants in this atrial cardiomyopathy pedigree. Because of failure to find any promising mutations in the 2 genes previously associated with atrial standstill, *SCN5A* and *GJA5*,[18] we performed exome sequencing in 2 patients, II-1 and II-3. In total, 62 960 single-nucleotide variants and 4192 insertions/deletions (Indels) were detected after stringent quality control using KGGSeq (V0.8),[12] and we chose the top 60 single-nucleotide variants (listed in Table S4) for validation according to their predicted pathogenic probability.[19] It turned out that 2 missense single-nucleotide variants (c. 610G>C of *TUBG2* and c. 31G>A of *MYL4*) in 17q21 perfectly cosegregated with the dominant inheritance mode in the pedigree. To further map the specific linkage regions in 17q21, the multipoint parametric linkage analysis in 17q21 provided a maximal logarithm of the odds score of 5.3 (Figure 2A). Haplotype analysis showed a ≈6 Mbp (or ≈5 cM) region exclusively shared by patients.

Based on bioinformatic analysis, both GeneWanderer and Endeavour ranked *MYL4* in the top 2 genes in terms of its functional relationship to *SCN5A* and *GJA5* (listed in Tables S5 and S6). Importantly, the identified missense mutation c. 31G>A in *MYL4* changed the negatively charged residue (glutamic acid) to a positively charged 1 (lysine), *p.E11K*. This

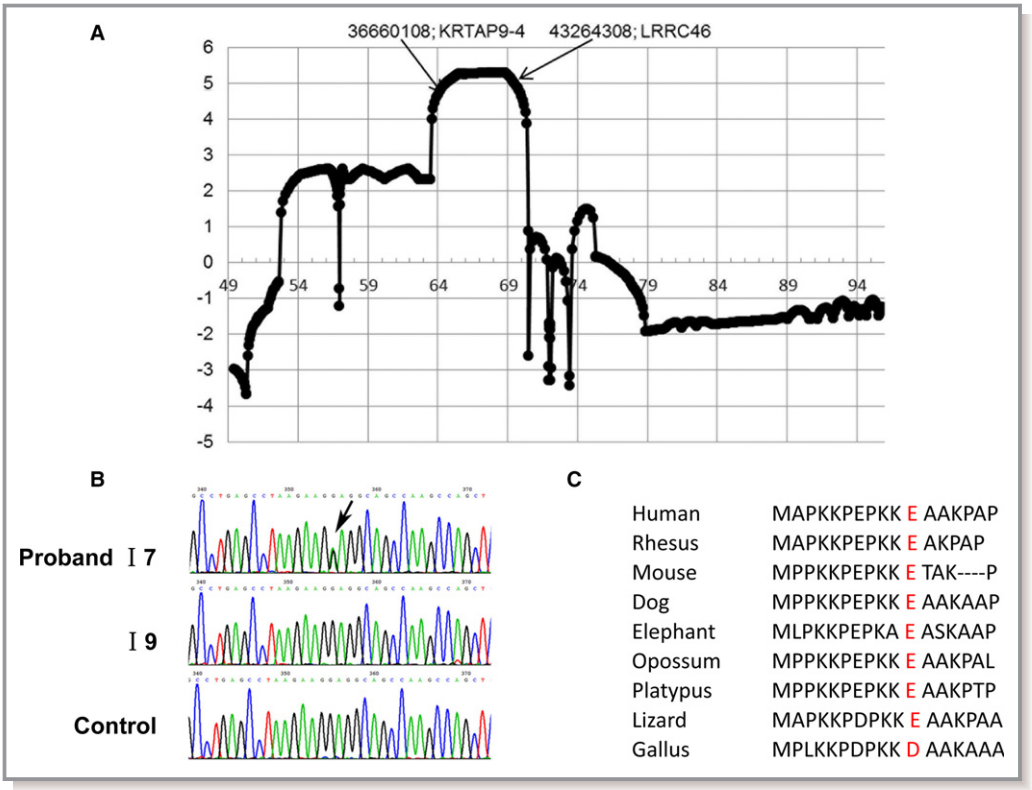

Figure 2. Genetic analysis. A, The multiple linkage analysis logarithm of the odds score in 17q21. B, Mutation (31G>A) in *MYL4* confirmed by Sanger sequencing. C, The mutated locus is highly conserved across species. MYL4 indicates myosin light-chain 4.

mutation was predicted to be pathogenic by KGGSeq (V0.8) under a combined prediction model[19] of multiple deleteriousness and conservation scores (including SIFT,[20] MutationAssessor,[21] and GERP++[22]). The *MYL4* mutation was confirmed in the entire pedigree by Sanger sequencing (Figure 2B). The mutation corresponded positionally to a negatively charged amino acid that is highly conserved across species (Figure 2C).

Of note, all 6 affected individuals carried the *MYL4* mutation, and none of 38 nonaffected family members that were sequenced showed the mutation. There were 3 additional family members (I-1, I-5, and the father of I-7), who also had a history of bradycardia, but for whom neither DNA for sequencing nor sufficient clinical data to assess the precise phenotype were available.

MYL4 p.E11K Rats Show an Atrial Cardiomyopathy Phenotype

To assess the pathogenic contribution of the *MYL4 p.E11K* mutation, we constructed a knock-in *MYL4 p.E11K* rat model with CRISPR/Cas-mediated genome editing (Figure 3A and 3B). The P-wave amplitude of *MYL4 E11K*$^{+/-}$ and *MYL4 E11K*$^{+/+}$ rats decreased progressively, accompanied by prolongation of the PR interval, from 15 days of age. The phenotype was more severe in homozygous rats, with 40% of *MYL4 E11K*$^{+/+}$ rats losing their P wave by 3 months of age and 80% at 6 months. Nevertheless, heterozygote (*MYL4 E11K*$^{+/-}$) rats also showed a clear phenotype, albeit less dramatic compared with homozygotes, with reduced P-wave amplitude (Table S7) and left atrial dilation (Table S8) versus wild type (WT). The QRS duration was similar among all groups, indicating atrial-specific electrical pathology (Figure 3C through 3E; Table S7). No spontaneous atrial arrhythmias were observed in knock-in rats during routine ECG recording.

Echocardiography showed left atrial dilation (Figure 3F) in both *MYL4 E11K*$^{+/-}$ and *MYL4 E11K*$^{+/+}$ rats at 3 months and progressive increases with aging (Table S8). For example, at 6 months, left atrial diameters were 4.5±0.3 mm in *MYL4 E11K*$^{+/+}$ and 3.8±0.1 mm in *MYL4 E11K*$^{+/-}$ rats, compared with 3.2±0.1 mm in WT (P<0.001; Figure 3F through 3H; Table S8).

In contrast to the clear atrial changes, right and left ventricular chamber sizes and ejection fraction were similar among the 3 genotypes, with no deviation greater than 20% and a small change of borderline statistical significance only at 3 months in *MYL4 E11K*$^{+/+}$ rats. There were no differences

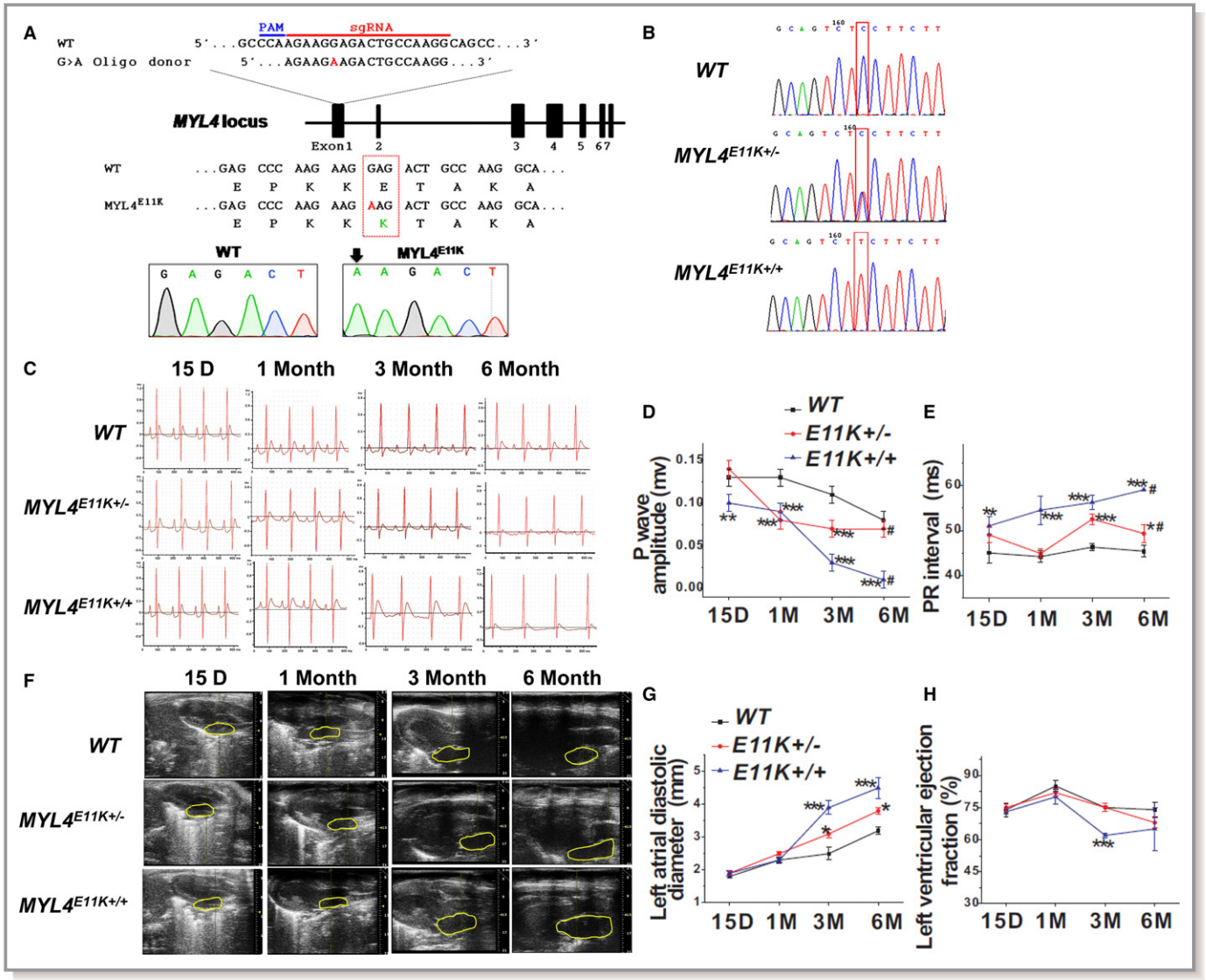

Figure 3. *MYL4 p.E11K* rat targeting strategies and atrial cardiomyopathic phenotype. A and B, The *MYL4 p.E11K* rat model was produced using CRISPR/Cas-mediated genome editing. The genotypes were confirmed by Sanger sequencing. C, Representative ECGs from WT, heterozygous, and homozygous *MYL4 E11K* rats at different ages. D and E, Mean data for P-wave amplitude and PR interval. P-wave amplitude of *MYL4 E11K*$^{+/-}$ rats progressively decreased, with prolongation of the PR interval, from 15 days of age. WT Rats: N=9; *MYL4 E11K*$^{+/-}$ rats: N=15; *MYL4 E11K*$^{+/+}$ rats: N=10. F, Representative echocardiographic images from 3 rat genotypes. G and H, Mean data for left atrial dimension and left ventricular ejection fraction. The left atria progressively enlarged in both *MYL4 E11K*$^{+/-}$ and *MYL4 E11K*$^{+/+}$ rat hearts, starting at 3 months of age. For TTE, 4 to 5 rats/group were averaged. Data are mean±SEM. **P*<0.05; ***P*<0.01; ****P*<0.001 vs WT, $^{\#}$*P*<0.05 among 15 days, 1 month, 3 months, and 6 months rats. ECG indicates standard 12-lead electrocardiography; MYL4, myosin light-chain 4; N, number; TTE, transthoracic ultrasound; WT, wild type.

in growth parameters among the 3 genotypes in either male or female rats (Figure S2).

Atrial Fibrosis and Cardiomyocyte Apoptosis in *MYL4 p.E11K* Rats

To further assess the atrial remodeling caused by *p.E11K* mutation, we collected atrial tissues from WT, *MYL4 E11K*$^{+/-}$ and *MYL4 E11K*$^{+/+}$ rats at ages of 2 days, 15 days, 1 month, 3 months, and 6 months. Left atrial fibrosis was quantified with Masson trichrome staining. *MYL4 E11K*$^{+/-}$ and *MYL4 E11K*$^{+/+}$ rats developed progressive left atrial fibrosis compared with WT rats, with statistically significant increases noted as early as 2 days of age (Figure 4A). At 2 days, 16.4±0.7% fibrous tissue content was observed in *MYL4 E11K*$^{+/+}$ rats and 8.4±1.5% in *MYL4 E11K*$^{+/-}$ rats, compared with 5.6±0.6% in WT (*P*<0.001). At 6 months old, 27.6±5.8% fibrosis was observed in *MYL4 E11K*$^{+/+}$ rats and 12.0±1.0% in *MYL4 E11K*$^{+/-}$ rats versus 8.7±0.6% in WT (*P*=0.016; Figure 4A and 4B).

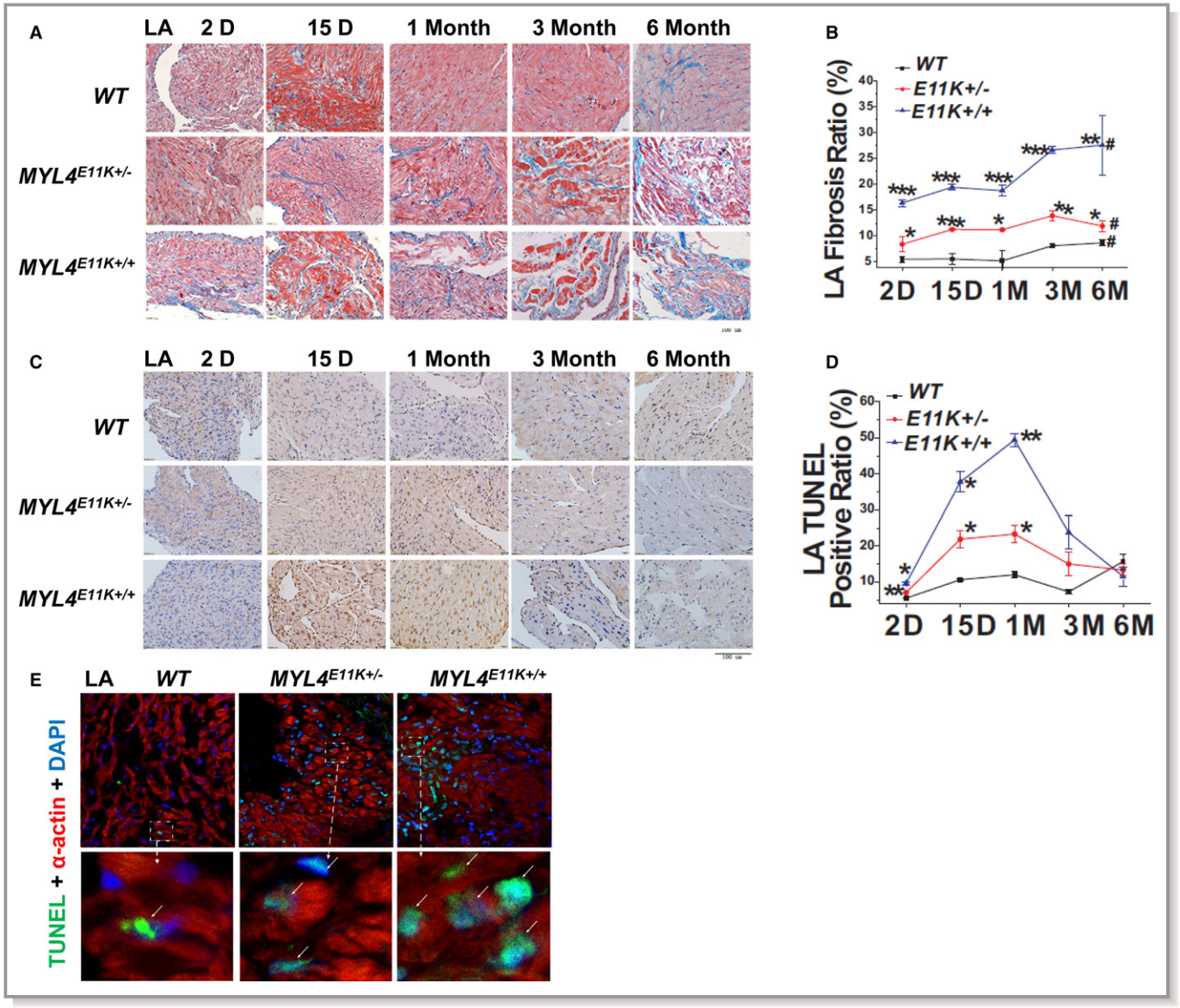

Figure 4. *MYL4 p.E11K* causes atrial fibrosis and cardiomyocytes apoptosis. A and B, Atrial fibrosis obtained by Masson staining was averaged for 4 to 5 hearts per group (6–10 fields per heart for each group). C and D, Representative images and mean data for TUNEL staining of atrial sections (4–5 hearts per group, 6–10 fields per heart for each group) from WT, *MYL4 E11K*$^{+/-}$, and *MYL4 E11K*$^{+/+}$rats. E, Confocal immunofluorescence showed that TUNEL-positive cells costained with α-actin, indicating that they were cardiomyocytes. TUNEL-positive staining is green. Nuclei are stained with DAPI (blue). Myocytes are stained for α-actin (red). Arrows indicate TUNEL-positive nuclei. Values are mean±SEM. **P*<0.05; ***P*<0.01; ****P*<0.001 vs WT;, $^{\#}$*P*<0.05 among 15 days, 1 month, 3 months, and 6 months rats. DAPI indicates 4′,6-diamidino-2-phenylindole; LA, left atrial; MYL4, myosin light-chain 4; TUNEL, terminal deoxynucleotidyl transferase dUTP nick end labeling; WT, wild type.

Reparative fibrosis typically replaces cardiomyocytes that have been lost through apoptosis or necrosis.[23,24] The proportion of terminal deoxynucleotidyl transferase dUTP nick end labeling–positive nuclei was significantly increased in atrial tissue of heterozygous and homozygous *MYL4 p.E11K* rats compared with WT, even at 2 days of age (Figure 4C and 4D). Confocal immunofluorescence showed that terminal deoxynucleotidyl transferase dUTP nick end labeling–positive cells appeared to also costain with α-actin (Figure 4E). We also performed proliferating cell nuclear antigen staining to obtain an index of fibroblast numbers. The percentage of proliferating cell nuclear antigen–positive nuclei increased significantly in atrial tissue for both *MYL4 E11K*$^{+/-}$ and *MYL4 E11K*$^{+/+}$ rats at day 15 (*P*<0.001; Figure S3A and S3B).

There were no differences among WT, *MYL4 E11K*$^{+/-}$ rat and *MYL4 E11K*$^{+/+}$ rats in atrial or ventricular cardiomyocyte size, based on FITC-conjugated wheat germ agglutinin staining (Figure S4). Similarly, there were no differences in ventricular

fibrous tissue content, apoptosis, or proliferating cell nuclear antigen–positive cell content among genotypes (Figures S3C, S3D, and S5).

Activation of Profibrotic and Proapoptotic Signals in the *p.E11K* Cardiomyocytes In Vivo and In Vitro

Atrial fibrosis can result from the activation of a variety of fibroproliferative signaling pathways.[25,26] Both small mothers against decapentaplegic and c-Jun N-terminal kinase phosphorylation was significantly increased in *MYL4 E11K*$^{+/+}$ (but not *MYL4 E11K*$^{+/-}$) atria (Figure 5A through 5C). Both *MYL4 E11K*$^{+/+}$ and *MYL4 E11K*$^{+/-}$ atria expressed significantly stronger expression of proapoptotic proteins B-cell lymphoma 2–associated X protein and Caspase-3 compared with WT (Figure 5D through 5G).

To independently assess the direct effects of the *MYL4* mutation on cardiomyocytes, we exposed cultured neonatal rat cardiomyocytes to WT MYL4 or MYL4^{E11K} overexpression by adenovirus-mediated gene transfer in vitro (Figure 6A through 6C). Neonatal rat cardiomyocytes overexpressing MYL4^{E11K} showed increased apoptosis compared with WT (Figure 6D and 6E), along with upregulation of the proapoptotic protein, caspase-3, and downregulation of the antiapoptotic protein, B-cell lymphoma 2 (Figure 6F through 6I). In addition, MYL4^{E11K} overexpression also increased small mothers against decapentaplegic and c-Jun N-terminal kinase phosphorylation relative to MYL4-WT (Figure 6F, 6J, and 6K). These data suggest that *MYL4 p.E11K* directly induces atrial profibrotic and proapoptotic signaling.

MYL4 protein expression decreased in *MYL4 p.E11K* knock-in rats compared to WT rats (Figure S6), and E11K protein overexpression in cultured neonatal rat cardiomyocytes reduced MYL4 protein levels (Figure 6A), suggesting that *MYL4 p.E11K* causes a loss of MYL4 protein stability and that this effect contributes to loss of function.

Atrial Arrhythmia and Heart Function in *MYL4 KO* Rats

To further assess the functional contribution of *MYL4*, we constructed a *MYL4* knockout rat model (for gene editing strategy, see Figure S6). *MYL4* knockout eliminated detectable MYL4 protein on western blot. Note that *MYL4 p.E11K* knock-in similarly reduced MYL4 protein expression, pointing to loss of protein stability (Figure S6). *MYL4 KO* rats

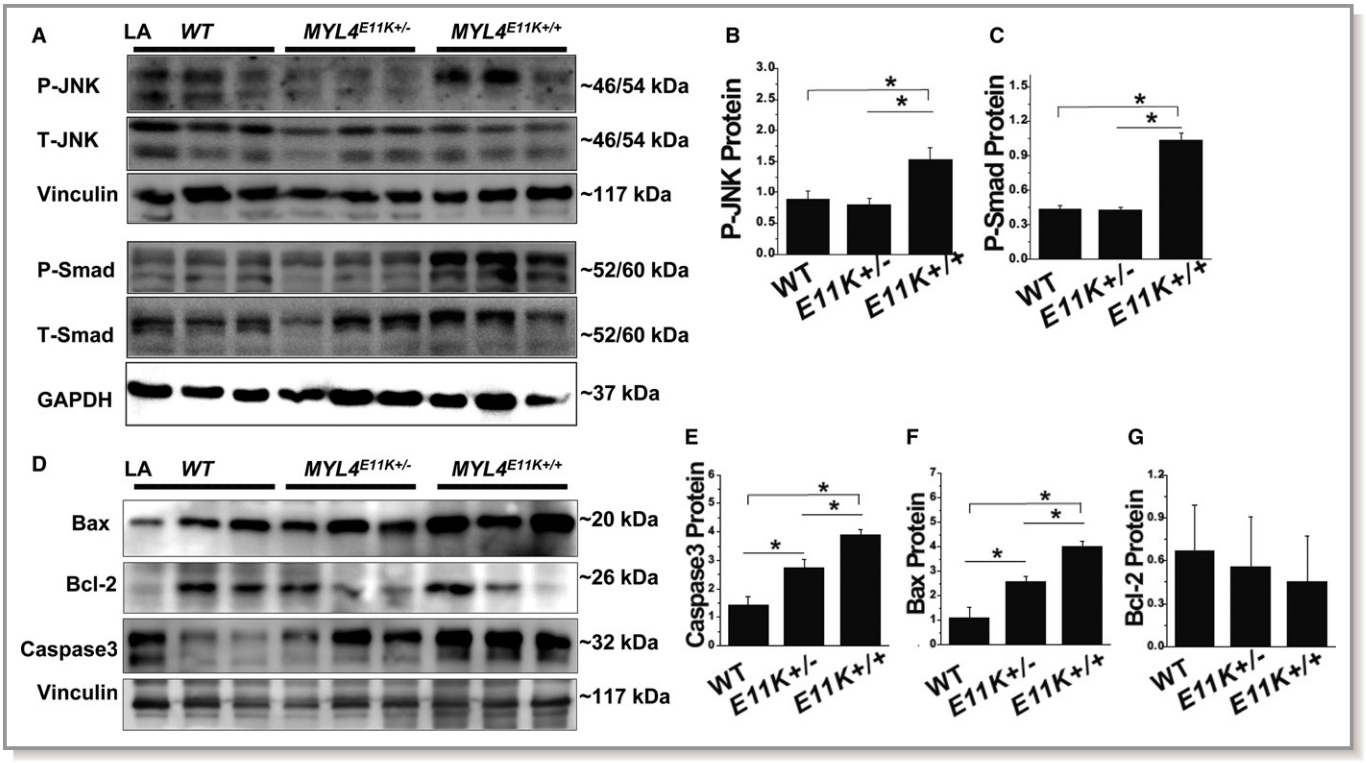

Figure 5. Profibrotic and proaptotic signaling. A through C, Western blots and mean data for JNK and Smad signaling in atria from WT, *MYL4 E11K*$^{+/-}$, and *MYL4 E11K*$^{+/+}$rats. D through G, Western blots and mean data for Bax and Caspase-3 expression in atria from WT, *MYL4 E11K*$^{+/-}$, and *MYL4 E11K*$^{+/+}$rats. Data are mean±SEM. Protein from 3 independent rat atrial samples were subjected to immunoblot for each groups. **P*<0.05. Bax indicates B-cell lymphoma 2–associated X protein; Bcl-2, B-cell lymphoma 2; JNK, c-Jun N-terminal kinase; LA, left atrial; MYL4, myosin light-chain 4; Smad, small mothers against decapentaplegic; WT, wild type.

demonstrated a similar phenotype to *MYL4 p.E11K* rats, but the phenotype manifested earlier and was more severe. Some homozygous *MYL4 KO* lost their P wave as early as 1 month of age. Overall, P-wave amplitudes decreased significantly in homozygous *KO* rats at the age of 1 month, whereas the PR interval increased (see Figure 7A through 7C; Table S9). On routine ECG recording, homozygous rats also showed spontaneous atrial arrhythmias, including atrial tachycardias, AF, and atrial standstill (Figure 7D; Table S9). Heterozygous *KO* rats (*MYL4 HT*) also showed atrial electrical conduction disorders as they aged (Figure 7A through 7D; Table S9). Echocardiography showed left atrial dilation in *KO* rats (8.7±2.2 mm in *KO* rats versus 5.4±0.1 mm in WT; $P<0.001$; Figure 7E and 7F; Table S10). *KO* rats also showed progressive atrial fibrosis (Figure 7H and 7I) and lost almost all contractile force generation (Figure S7). In vitro, MYL4 knockdown in cultured myocytes led to a similar myocyte death phenotype to *MYL4 p.E11K* overexpression (Figure S8), suggesting that loss of MYL4 function causes cell death that likely contributes to the progressive atrial cardiomyopathy phenotype.

Though there was no difference in ventricular fibrosis among WT, *MYL4 HT*, and *MYL4 KO* rats (Figure S9A and S9B), moderate statistically significant decreases in left ventricular function were noted in 6-month-old *MYL4 KO* rats, which may have been attributed to atrial arrhythmia and/or atrial structural and contractile remodeling (Figure 7G; Table S10).

Effects on Myosin ATPase Activity

In order to assess the molecular signature of MYL4 dysfunction, we constructed 3 types of recombinant plasmids: (1) pcDNA3.1-*MYL4*-GG (WT); (2) pcDNA3.1-*MYL4*-AA (the E11*K* mutation); and (3) pcDNA3.1-*MYL4*-12bp del (the *Del*, with 4 consecutive amino acids deleted near the *MYL4 p.E11* site), then expressed and purified the corresponding proteins in yeast. MYL4 modulates actin-activated ATPase activity,[5] and the ATPase activities of different proteins were analyzed based on the Km and Vmax of myosin. Both Km and Vmax were significantly smaller in the presence of MYL4-E11K protein than MYL4-WT protein (Figure S10). MYL4-Del protein did not affect myosin ATPase activity (Figure S10). These results indicate that the MYL4-E11K mutant protein specifically reduces the activity of myosin ATPase.

To relate effects on myosin ATPase activity to atrial remodeling and obtain an additional control for the specificity of the *MYL4 p.E11K* mutation, we constructed an additional rat model, with the same 4 consecutive amino-acid deletion near the *MYL4 p.E11K* site (Figure S6A and S6C). Neither $MYL4^{del+/-}$ nor $MYL4^{del+/+}$ rats showed atrial or ventricular fibrosis, arrhythmia, or structural remodeling (Figure 8 and Figure S9C and S9D; Tables S11 and S12), indicating that mutations in the gene that do not affect myosin function do not cause atrial cardiomyopathy.

Discussion

In this study, we first identified the missense mutation, c.31G>A (*p.E11K*), as a candidate causal gene variant for atrial cardiomyopathy through genetic analysis of a large family with atrial standstill. We then confirmed the role of this mutation with the use of a series of novel rat models generated by CRISPR/Cas-mediated genome editing. We found that normal MYL4 function is essential for atrial electrical, contractile, and structural integrity. MYL4 dysfunction, whether as a result of knockout or targeted knock-in of the human mutation, causes early atrial fibrosis associated with enhanced proaptotoic and profibrotic signaling, associated with an atrial cardiomyopathy featuring atrial arrhythmia, atrial contractile failure, and atrial enlargement.

Relationship to Past Studies of *MYL4* Gene-Variant–Associated Atrial Disease

Orr et al recently described a family with early-onset AF and an apparently causal *MYL4* mutation, p.Glu11Lys.[8] Interestingly, this mutation results in the same E11K amino-acid alteration that we observed in our kindred. This is a highly nonconservative mutation of an acidic to a basic amino acid, with the potential to strongly alter protein function. Affected individuals had early-onset AF, evidence of atrial contractile dysfunction and conduction abnormalities requiring pacemaker insertion, a very similar clinical presentation to our patients. Gudbjartsson et al very recently identified a frameshift deletion in *MYL4* causing AF at an early age, pacemaker requirement, and a high incidence of stroke.[7] The clinical features were predominantly atrial, but signs of mild ventricular dysfunction eventually developed, primarily in the fifties and sixties. The clinical features of affected patients in the reports by Orr et al and Gudbardtsson et al were similar overall to those of our patients. As in our patients, inheritance appeared to be dominant in the Orr kindred,[8] whereas it was recessive in the Gudbjartsson study.[7]

The only previous animal-model data relating to these *MYL4* gene variants come from the Orr study,[8] in which the investigators reproduced the orthologous mutation (E17K in *cMLC-1*) in zebrafish. They noted abnormal sinoatrial impulse generation and bradycardia, along with prolonged P-wave duration and atrial enlargement. They noted marked disruption of sarcomere structure as early as 5 days postfertilization with loss of Z-discs.

Here, we created novel rat models of MYL4 dysfunction with the use of CRISPR/Cas gene editing. The affected rats

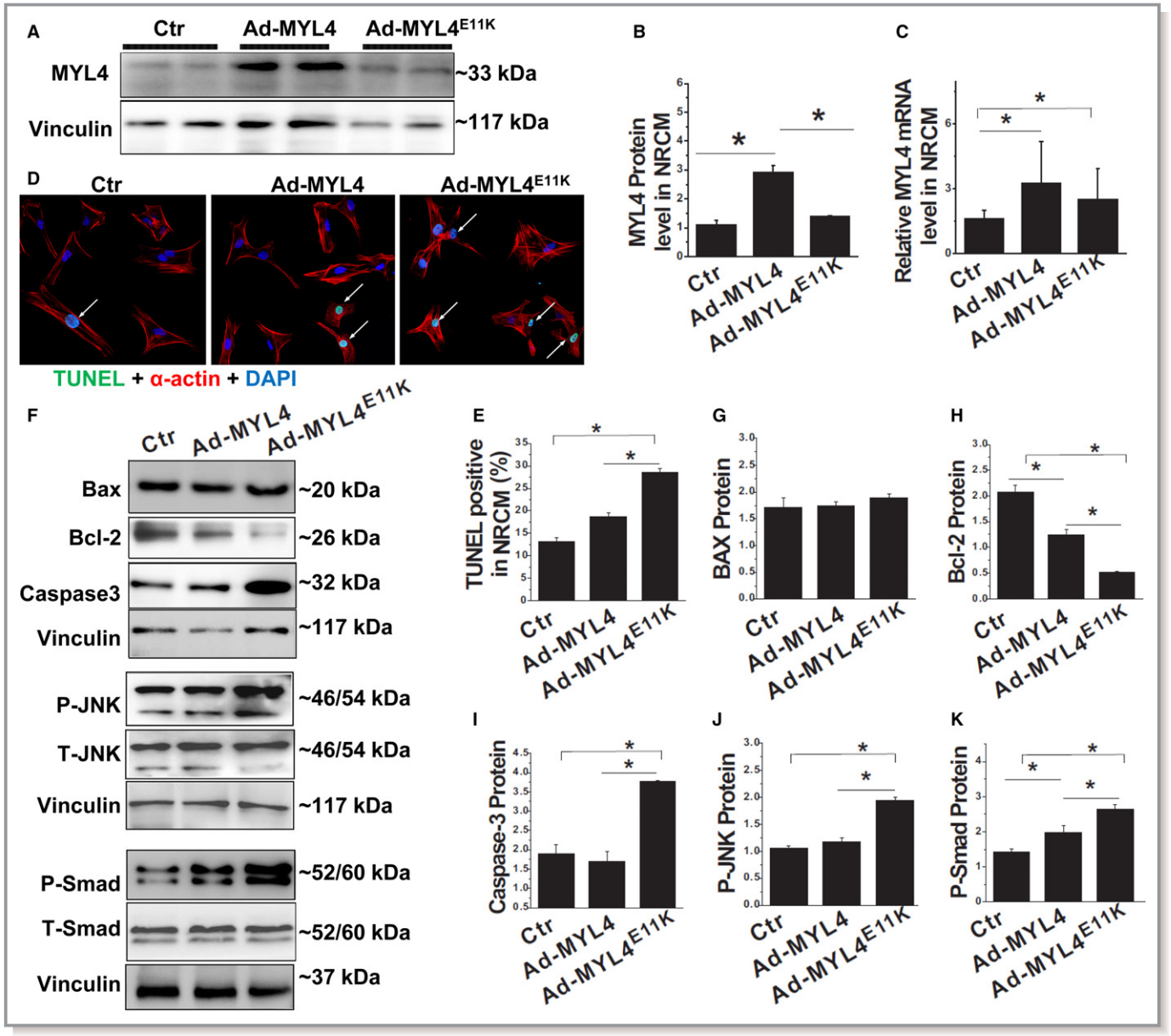

Figure 6. Acute *MYL4 p.E11K* gene transfer causes NRCM apoptosis and activates profibrotic signaling. A through C, Western blot and quantitative RT-PCR analysis of *MYL4* expression in NRCM exposed to gene transfer with different adenoviral constructs. D and E, Cardiomyocytes exposed to *MYL4 E11K* adenovirus showed significantly greater TUNEL-positivity compared with WT. TUNEL-positive staining is FITC (green). Nuclei are stained with DAPI (blue). Myocytes are stained for α-actin (red). Arrows indicate TUNEL-positive nuclei. F through K, Western blot analysis for proapoptotic protein caspase-3 and antiapoptotic protein Bcl-2 (F through I) and Smad/JNK signaling. Data are mean±SEM. The sample sizes were N=3 NRCM isolations per group with n=3 replicates from each isolate for each experiment. **P*<0.05. Bax indicates B-cell lymphoma 2–associated X protein; Bcl-2, B-cell lymphoma 2; Ctr indicates control; DAPI, 4′,6-diamidino-2-phenylindole; JNK, c-Jun N-terminal kinase; MYL4, myosin light-chain 4; N, number; NRCM, neonatal rat cardiomyocytes; Smad, small mothers against decapentaplegic; TUNEL, terminal deoxynucleotidyl transferase dUTP nick end labeling; WT, wild type.

confirmed the ability of MYL4 dysfunction, whether by knockout or by knock-in of a gene variant reproducing the clinical E11K mutation, to produce the cardinal clinical features of atrial electrical dysfunction, loss of atrial contractility, and atrial dilation constituting a highly atrial-selective cardiomyopathy. Proapoptotic and profibrotic signaling were enhanced in knock-in rats, and this appeared to be a direct result of the mutation rather than secondary to the atrial cardiomyopathy phenotype, because in vitro gene transfer of the mutation into neonatal rat cardiomyocytes reproduced the signaling changes. Interestingly, evidence of apoptosis and atrial fibrosis was present in vivo as early as 2 days of age (Figure 4), well before substantial loss of P-wave amplitude or increase in left atrial dimension (Figure 3). These observations

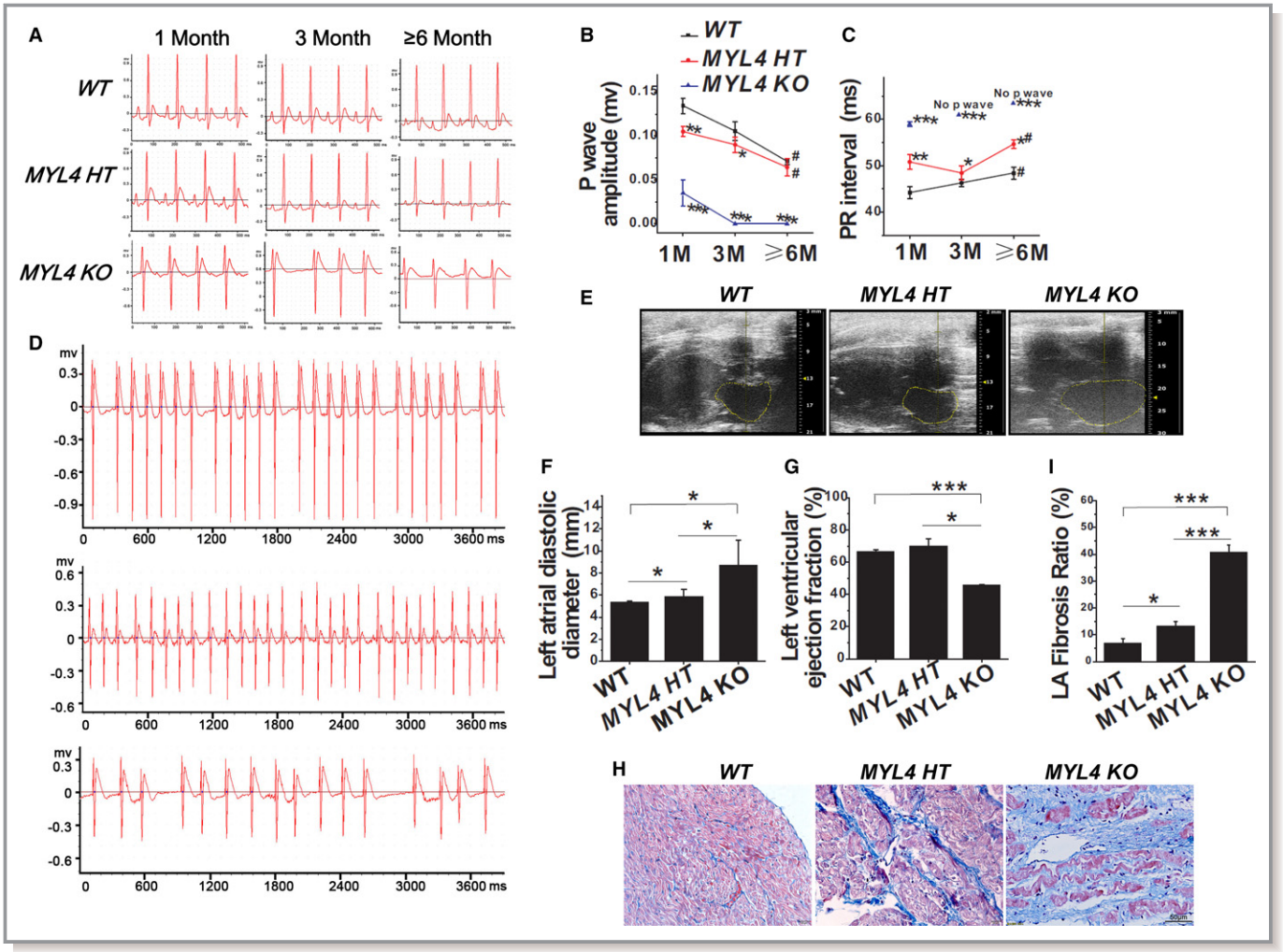

Figure 7. Atrial cardiomyopathy phenotype in *MYL4 KO* rats. A, Representative ECGs for WT, heterozygous, and homozygous *MYL4 KO* rats at different ages. B and C, Mean data for P-wave amplitude and PR interval. WT Rats: N=9; *MYL4 HT* rats: N=12; *MYL4 KO* rats: N=5. D, Typical spontaneous atrial arrhythmias. E through G, Echocardiography showed left atrial enlargement in *KO* rats. WT Rats: N=3; *MYL4 HT* rats: N=5; *MYL4 KO* rats: N=3. H and I, *KO* rats developed atrial fibrosis (4–5 hearts per group, 6–10 fields per heart for each group). Data are mean±SEM. **P*<0.05; ***P*<0.01; ****P*<0.001 vs WT; #*P*<0.05 among 1 month, 3 months, and ≥6 months rats. ECG indicates standard 12-lead electrocardiography; HT, heterozygous; KO, knockout; MYL4, myosin light-chain 4; N, number; WT, wild type.

are consistent with the notion that Z-disc disruption affects the many macromolecular complexes involved in intracellular signaling that are located at the Z-disc,[8,27] producing profound atrial cardiomyocyte remodeling. Unlike the zebrafish, in which the orthologous gene is expressed in both the atria and ventricles, in rats and humans MYL4 shows strong atrial-selective expression, consistent with the atrial-selective phenotype noted.

Both in clinical reports[7] and in our rats, some evidence of ventricular dysfunction appeared later in life. Ventricular dysfunction may be a secondary consequence of atrial arrhythmias, bradycardia, and dyssynchronous contraction caused by the primary atrial cardiomyopathy, or may be attributed to ventricular consequences of the mutation related to a return of ventricular MYL4 expression because of cardiac dysfunction.[4]

Insights Into Atrial Cardiomyopathy

The term "atrial cardiomyopathy" first appeared in the literature in 1972.[28] Kottkamp has argued that many cases of AF may be attributed to an underlying "atrial fibrotic cardiomyopathy".[2,29] Recently, a consensus has emerged, defining and characterizing the concept of atrial cardiomyopathy.[1] Insights from genetic paradigms greatly contributed to our understanding of ventricular cardiomyopathies,[30] but very little information has been available to date about genetic causes of atrial cardiomyopathy. Our identification of a

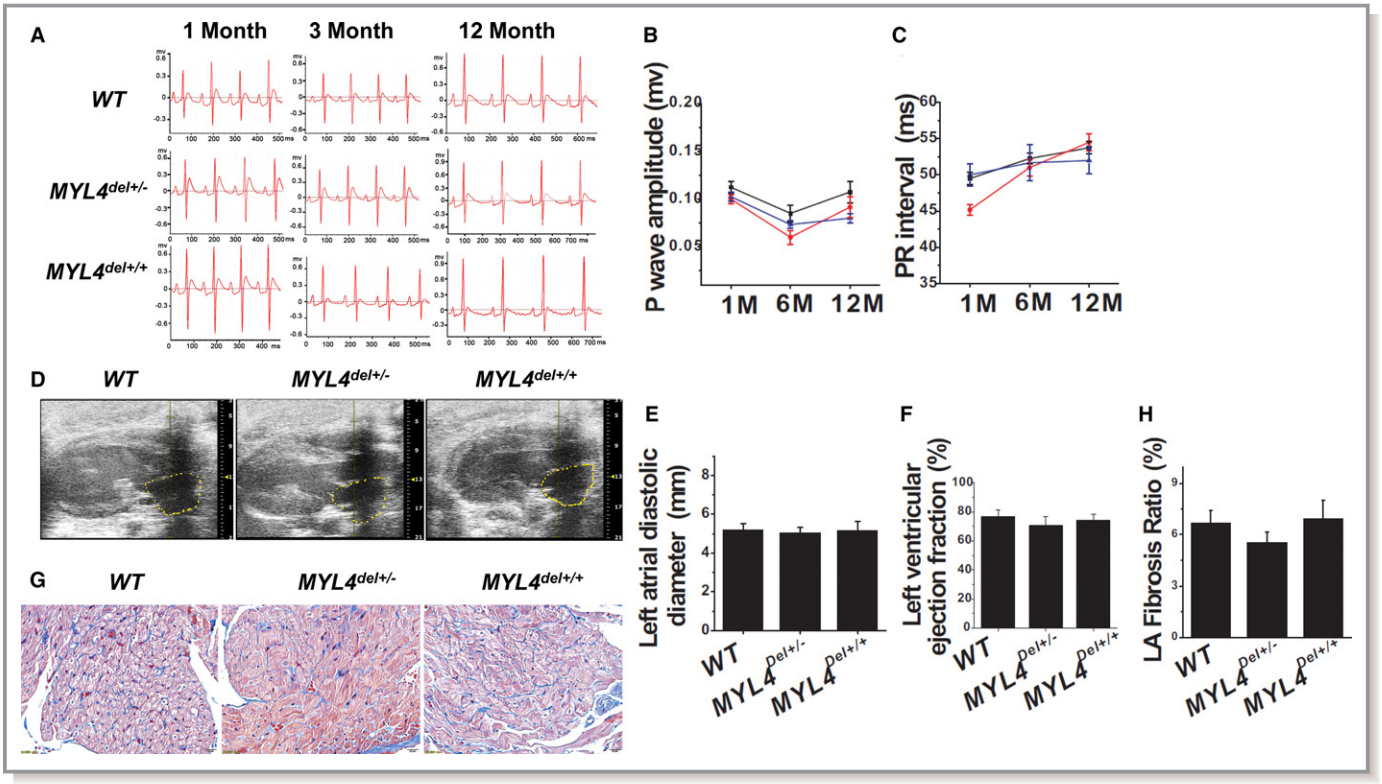

Figure 8. *MYL4 del* mutation rats do not show atrial cardiomyopathy. A through C, ECG data for WT (N=4), heterozygous, and homozygous *MYL4 deletion mutation* rats at different ages. Neither the $MYL4^{del+/-}$ (N=5) nor $MYL4^{del+/+}$ (N=4) rats had significant arrhythmia. D through F, Echocardiography showed the absence of structural remodeling in $MYL4^{del+/-}$ and $MYL4^{del+/+}$ rats. WT Rats: N=3; $MYL4^{del+/-}$ rats: N=5; $MYL4^{del+/+}$ rats: N=3. G and H, Neither the $MYL4^{del+/-}$ nor $MYL4^{del+/+}$ rats had significant atrial fibrosis (4–5 hearts per group, 6–10 fields per heart for each group). ECG indicates standard 12-lead electrocardiography; MYL4, myosin light-chain 4; N, number; WT, wild type.

pathological *MYL4* mutation causing atrial cardiomyopathy and the development of powerful new animal models with which to study its pathophysiology is a step forward in the understanding of atrial cardiomyopathy. Atrial fibrosis appears to be a very early development in the evolution of this model. Along with the direct activation of proapoptotic and profibrotic signaling by gene transfer of the pathogenic mutation in vitro, these results point to this entity as a prototype for fibrotic atrial cardiomyopathy and provide insights into the underlying mechanisms. Prominent pathological features include highly atrial-selective cardiomyocyte apoptosis and tissue fibrosis (eg, see Figure 4). According to the EHRA/HRS/APHRS/SOLAECE expert consensus, our rat model would be classified as a type III atrial cardiomyopathy, which combines cardiomyocyte pathology and fibrosis.[1]

Clinical Relevance

Clinically, atrial cardiomyopathy caused by *MYL4* mutation progressed gradually in our patients: Despite sinus rhythm at a young age, contractile abnormalities were already evident, followed by atrial arrhythmia, atrioventricular block, and finally total atrial standstill. In the early stage of the condition, the ECG may appear normal and patients may have negligible symptoms. Nevertheless, TTE indicates reduced mechanical activity in the atria, implying that TTE may be a useful technique for the early identification of affected individuals in a disease-bearing kindred.

Besides the specific rare familial entity we studied, our work can provide broader insights into the development of atrial cardiomyopathy. Signaling events of the type we identified have also been noted in various acquired forms of atrial cardiomyopathy.[31] Further study in our rat models might allow for the identification of vulnerable molecular targets in atrial cardiomyopathy development that could produce new therapeutic approaches.

Potential Limitations

The phenotype of *MYL4* mutated or *KO* rats directly paralleled the ECG changes and atrial dysfunction that we observed in our patients. *MYL4 p.E11K* rats had evidence of apoptosis and atrial fibrosis at an early stage. Although the phenotype of *KO* rats was similar overall to that of the *MYL4 p.E11K* rats, it was generally more severe and developed faster. Atrial tachyarrhythmias were easily noted in *KO* rats, but were not

apparent in the *MYL4 p.E11K* knock-in animals. The greater susceptibility of *KO* rats may be attributed to their complete loss of MYL4 function. The absence of atrial tachyarrhythmias in knock-in rats may be attributed to the fact that the only rhythm recordings available to us were standard ECGs; continuous telemetry might have revealed spontaneous arrhythmias. Although the phenotype of the knock-in rats was similar to that of our patients, there were some differences, most notably in the occurrence of spontaneous arrhythmias. Some of the discrepancy may be attributed to the absence of extended rhythm recording in the rats. Alternatively, background genetic control may play a role in conditioning the phenotype and promoting atrial arrhythmogenesis in humans. Nevertheless, *KO* rats did manifest spontaneous atrial tachyarrhythmias, confirming the principle that MYL4 dysfunction is, by itself, sufficient to cause atria arrhythmogenesis.

The underlying molecular mechanism of the myosin ATPase activity reduction is complex. Force production is considered to be associated with the Pi release step and the transition from weakly (non-force-generating) to strongly attached (force-generating) states.[32] Both Km and Vmax of myosin head ATPase are lower in the MYL4-E11K protein than MYL4-WT protein.

The work provided in this article presents a novel model with which to study the MYL4-mutation–related atrial cardiomyopathy and characterizes the model in relationship to the clinical presentation. However, the precise mechanisms underlying key processes like apoptotic cell death and atrial fibrosis in this model remain to be determined in future studies.

Conclusions

We have shown, with the use of novel genetically defined rat models, that MYL4 is essential for atrial electrical, functional, and structural integrity, and that MYL4 dysfunction can account for severe inherited atrial cardiomyopathy in an extended kindred. We have obtained evidence that atrial apoptotic cell death and fibrosis are very early findings and are apparent before any functional manifestations of atrial cardiomyopathy. These observations are consistent with an important pathophysiological role for enhanced proapoptotic and profibrotic signaling that is activated rapidly in the presence of the causative mutation. These biological findings have the potential to advance our understanding of the molecular basis of atrial cardiomyopathy and eventually to lead to new diagnosis and therapeutic modalities.

Sources of Funding

This work was supported by Chinese National Natural Science Foundation No. 81270256, 81370391, 81470394, and 81670230; Shanghai Sailing Program No. 15YF1409400; Hong Kong Research Grants Council GRF HKU 776412M, Hong Kong Research Grants Council Theme-Based Research Scheme T12-705/11; European Community Seventh Framework Programme Grant on European Network of National Schizophrenia Networks Studying Gene-Environment Interactions (EU-GEI); the HKU Seed Funding Programme for Basic Research 201302159006; the Health and Medical Research Fund 01121436; the Canadian Institutes of Health Research; and the Heart and Stroke Foundation of Canada.

Acknowledgments

We thank the patients and family members for taking part in this study.

Disclosures

None.

References

1. Goette A, Kalman JM, Aguinaga L, Akar J, Cabrera JA, Chen SA, Chugh SS, Corradi D, D'Avila A, Dobrev D, Fenelon G, Gonzalez M, Hatem SN, Helm R, Hindricks G, Ho SY, Hoit B, Jalife J, Kim YH, Lip GY, Ma CS, Marcus GM, Murray K, Nogami A, Sanders P, Uribe W, Van Wagoner DR, Nattel S; Document Reviewers. EHRA/HRS/APHRS/SOLAECE expert consensus on atrial cardiomyopathies: definition, characterization, and clinical implication. *Europace*. 2016;18:1455–1490.
2. Kottkamp H. Human atrial fibrillation substrate: towards a specific fibrotic atrial cardiomyopathy. *Eur Heart J*. 2013;34:2731–2738.
3. Disertori M, Mase M, Marini M, Mazzola S, Cristoforetti A, Del Greco M, Kottkamp H, Arbustini E, Ravelli F. Electroanatomic mapping and late gadolinium enhancement MRI in a genetic model of arrhythmogenic atrial cardiomyopathy. *J Cardiovasc Electrophysiol*. 2014;25:964–970.
4. Hernandez OM, Jones M, Guzman G, Szczesna-Cordary D. Myosin essential light chain in health and disease. *Am J Physiol Heart Circ Physiol*. 2007;292:H1643–H1654.
5. Ho G, Chisholm RL. Substitution mutations in the myosin essential light chain lead to reduced actin-activated ATPase activity despite stoichiometric binding to the heavy chain. *J Biol Chem*. 1997;272:4522–4527.
6. Gudbjartsson DF, Helgason H, Gudjonsson SA, Zink F, Oddson A, Gylfason A, Besenbacher S, Magnusson G, Halldorsson BV, Hjartarson E, Sigurdsson GT, Stacey SN, Frigge ML, Holm H, Saemundsdottir J, Helgadottir HT, Johannsdottir H, Sigfusson G, Thorgeirsson G, Sverrisson JT, Gretarsdottir S, Walters GB, Rafnar T, Thjodleifsson B, Bjornsson ES, Olafsson S, Thorarinsdottir H, Steingrimsdottir T, Gudmundsdottir TS, Theodors A, Jonasson JG, Sigurdsson A, Bjornsdottir G, Jonsson JJ, Thorarensen O, Ludvigsson P, Gudbjartsson H, Eyjolfsson GI, Sigurdardottir O, Olafsson I, Arnar DO, Magnusson OT, Kong A, Masson G, Thorsteinsdottir U, Helgason A, Sulem P, Stefansson K. Large-scale whole-genome sequencing of the Icelandic population. *Nat Genet*. 2015;47:435–444.
7. Gudbjartsson DF, Holm H, Sulem P, Masson G, Oddsson A, Magnusson OT, Saemundsdottir J, Helgadottir HT, Helgason H, Johannsdottir H, Gretarsdottir S, Gudjonsson SA, Njolstad I, Lochen ML, Baum L, Ma RC, Sigfusson G, Kong A, Thorgeirsson G, Sverrisson JT, Thorsteinsdottir U, Stefansson K, Arnar DO. A frameshift deletion in the sarcomere gene MYL4 causes early-onset familial atrial fibrillation. *Eur Heart J*. 2017;38:27–34.
8. Orr N, Arnaout R, Gula LJ, Spears DA, Leong-Sit P, Li Q, Tarhuni W, Reischauer S, Chauhan VS, Borkovich M, Uppal S, Adler A, Coughlin SR, Stainier DY, Gollob MH. A mutation in the atrial-specific myosin light chain gene (MYL4) causes familial atrial fibrillation. *Nat Commun*. 2016;7:11303.
9. Woolliscroft J, Tuna N. Permanent atrial standstill: the clinical spectrum. *Am J Cardiol*. 1982;49:2037–2041.
10. Li H, Durbin R. Fast and accurate short read alignment with Burrows-Wheeler transform. *Bioinformatics*. 2009;25:1754–1760.
11. DePristo MA, Banks E, Poplin R, Garimella KV, Maguire JR, Hartl C, Philippakis AA, del Angel G, Rivas MA, Hanna M, McKenna A, Fennell TJ, Kernytsky AM,

Sivachenko AY, Cibulskis K, Gabriel SB, Altshuler D, Daly MJ. A framework for variation discovery and genotyping using next-generation DNA sequencing data. *Nat Genet*. 2011;43:491–498.

12. Li MX, Gui HS, Kwan JS, Bao SY, Sham PC. A comprehensive framework for prioritizing variants in exome sequencing studies of Mendelian diseases. *Nucleic Acids Res*. 2012;40:e53.
13. Sobel E, Lange K. Descent graphs in pedigree analysis: applications to haplotyping, location scores, and marker-sharing statistics. *Am J Hum Genet*. 1996;58:1323–1337.
14. Tranchevent LC, Barriot R, Yu S, Van Vooren S, Van Loo P, Coessens B, De Moor B, Aerts S, Moreau Y. ENDEAVOUR update: a web resource for gene prioritization in multiple species. *Nucleic Acids Res*. 2008;36:W377–W384.
15. Kohler S, Bauer S, Horn D, Robinson PN. Walking the interactome for prioritization of candidate disease genes. *Am J Hum Genet*. 2008;82:949–958.
16. Shao Y, Guan Y, Wang L, Qiu Z, Liu M, Chen Y, Wu L, Li Y, Ma X, Liu M, Li D. CRISPR/Cas-mediated genome editing in the rat via direct injection of one-cell embryos. *Nat Protoc*. 2014;9:2493–2512.
17. Li D, Qiu Z, Shao Y, Chen Y, Guan Y, Liu M, Li Y, Gao N, Wang L, Lu X, Zhao Y, Liu M. Heritable gene targeting in the mouse and rat using a CRISPR-Cas system. *Nat Biotechnol*. 2013;31:681–683.
18. Groenewegen WA, Firouzi M, Bezzina CR, Vliex S, van Langen IM, Sandkuijl L, Smits JP, Hulsbeek M, Rook MB, Jongsma HJ, Wilde AA. A cardiac sodium channel mutation cosegregates with a rare connexin40 genotype in familial atrial standstill. *Circ Res*. 2003;92:14–22.
19. Li MX, Kwan JS, Bao SY, Yang W, Ho SL, Song YQ, Sham PC. Predicting Mendelian disease-causing non-synonymous single nucleotide variants in exome sequencing studies. *PLoS Genet*. 2013;9:e1003143.
20. Kumar P, Henikoff S, Ng PC. Predicting the effects of coding non-synonymous variants on protein function using the SIFT algorithm. *Nat Protoc*. 2009;4:1073–1081.
21. Reva B, Antipin Y, Sander C. Predicting the functional impact of protein mutations: application to cancer genomics. *Nucleic Acids Res*. 2011;39:e118.
22. Davydov EV, Goode DL, Sirota M, Cooper GM, Sidow A, Batzoglou S. Identifying a high fraction of the human genome to be under selective constraint using GERP++. *PLoS Comput Biol*. 2010;6:e1001025.
23. Hanna N, Cardin S, Leung TK, Nattel S. Differences in atrial versus ventricular remodeling in dogs with ventricular tachypacing-induced congestive heart failure. *Cardiovasc Res*. 2004;63:236–244.
24. Cardin S, Li D, Thorin-Trescases N, Leung TK, Thorin E, Nattel S. Evolution of the atrial fibrillation substrate in experimental congestive heart failure: angiotensin-dependent and -independent pathways. *Cardiovasc Res*. 2003;60:315–325.
25. Nattel S, Dobrev D. Electrophysiological and molecular mechanisms of paroxysmal atrial fibrillation. *Nat Rev Cardiol*. 2016;13:575–590.
26. Burstein B, Nattel S. Atrial fibrosis: mechanisms and clinical relevance in atrial fibrillation. *J Am Coll Cardiol*. 2008;51:802–809.
27. Nattel S. Close connections between contraction and rhythm: a new genetic cause of atrial fibrillation/cardiomyopathy and what it can teach us. *Eur Heart J*. 2017;38:35–37.
28. Nagle RE, Smith B, Williams DO. Familial atrial cardiomyopathy with heart block. *Br Heart J*. 1972;34:205.
29. Kottkamp H. Fibrotic atrial cardiomyopathy: a specific disease/syndrome supplying substrates for atrial fibrillation, atrial tachycardia, sinus node disease, AV node disease, and thromboembolic complications. *J Cardiovasc Electrophysiol*. 2012;23:797–799.
30. Maron BJ, Towbin JA, Thiene G, Antzelevitch C, Corrado D, Arnett D, Moss AJ, Seidman CE, Young JB; American Heart Association; Council on Clinical Cardiology, Heart Failure and Transplantation Committee; Quality of Care and Outcomes Research and Functional Genomics and Translational Biology Interdisciplinary Working Groups; Council on Epidemiology and Prevention. Contemporary definitions and classification of the cardiomyopathies: an American Heart Association Scientific Statement from the Council on Clinical Cardiology, Heart Failure and Transplantation Committee; Quality of Care and Outcomes Research and Functional Genomics and Translational Biology Interdisciplinary Working Groups; and Council on Epidemiology and Prevention. *Circulation*. 2006;113:1807–1816.
31. Wakili R, Voigt N, Kääb S, Dobrev D, Nattel S. Recent advances in the molecular pathophysiology of atrial fibrillation. *J Clin Invest*. 2011;121:2955–2968.
32. Siemankowski RF, Wiseman MO, White HD. ADP dissociation from actomyosin subfragment 1 is sufficiently slow to limit the unloaded shortening velocity in vertebrate muscle. *Proc Natl Acad Sci U S A*. 1985;82:658–662.

Supplemental Material

Data S1. Supplemental Methods

1. Exome sequencing in two atrial standstill family members

We performed exome capture sequencing for two affected individuals II1 and II3 at the Beijing Genomics Institute in Shenzhen China (http://www.genomics.cn/). The qualified genomic DNA sample was randomly fragmented by Covaris and DNA fragments with a base pair peak of 150 to 200bp, and then adapters were ligated to both ends of the resulting fragments. The adapter-ligated templates were purified with Agencourt AMPure SPRI beads and fragments with insert size about 250 bp were excised. Extracted DNA was amplified by ligation-mediated PCR (LM-PCR), purified, and hybridized to the SureSelect Biotinylated RNA Library (BAITS) for enrichment: hybridized fragments were bound to the strepavidin beads whereas non-hybridized fragments were washed out after 24 hours. Captured LM-PCR products were subjected to Agilent 2100 Bioanalyzer to estimate the magnitude of enrichment. Each captured library was then loaded on the HiSeq 2000 platform for high-throughput exome sequencing with expected minimal coverage 30X at target regions. Raw image files were processed by Illumina Pipeline v1.6 for base-calling with default parameters and sequences were generated in paired-end 90-bp reads.

2. Calling and prioritization of exome sequence variants

The paired-end 90 bp short reads were mapped onto the UCSC human reference genome, version hg18 (corresponding to NCBI Build36), by BWA[1]. Duplicated reads were removed by Picard (http://picard.sourceforge.net/). The Genome analysis toolkit (GATK)[2] was used to recalibrate the alignments and to call single nucleotide variants (SNVs) and short insertion-deletion variants (Indels). All genotype calls with sequencing read coverage ≤8x, Phred-scaled mapping calling quality of ≤20, Phred-scaled base calling quality of ≤50, Phred-scaled genotype calling quality of ≤20, ≥5% reads carrying alternative alleles in reference homozygous genotypes, ≤25% reads carrying alternative alleles in heterozygous genotypes or Phred-scaled probability of the second candidate genotype ≤ 50 were excluded in quality control.

We prioritized the SNVs and Indels by multilayer resources and functions through KGGSeq,

i.e., Knowledge-based mining platform for Genomic and Genetic studies using Sequence data (http://statgenpro.psychiatry.hku.hk/kggseq). Specifically, we firstly excluded the following variants sequentially: those with homozygous genotypes in all affected family members and heterozygous in unaffected ones (incompatible with rare autosomal dominant inheritance under non-consanguineous mating), those with a frequency of over 0.005 in the 1000 Genome Project or dbSNP database or the NHLBI GO Exome Sequencing Project (4500) or an in-house exome sequencing dataset (from a sample of 100 Southern Chinese), those that do not alter proteins, and those that were predicted to be non-pathogenic based on deleteriousness scores[3]. The variants whose gene products have protein-protein interaction (PPI) with the protein of 2 suggested atrial-standstill causal genes, SCN5A and GJA5, were then prioritized, and variants with genes sharing the same biological pathways with either of the 2 genes were prioritized as well. Finally, in a prioritized short list of sequence variants, KGGSeq also automatically searched relevant publications, which mentioned the variants' genes and the disease name (atrial standstill) in the titles or abstracts in the NCBI PubMed database to provide more clues to link the variants with the disease.

3. Surface ECG and TTE

For surface ECG recording, rats were anesthetized with 1-2% isoflurane, diluted in 98-99% oxygen at a constant flow rate of 1 L/min and placed in a supine position on a heated platform to maintain a physiological temperature. The electrodes were inserted in the subcutaneous tissue of the forelimbs and left hind limb to produce Lead II recordings. The electrodes were connected to a biological signal acquisition amplifier (BL-420S, Taimeng Co, Chengdu, China). Upon completion of electrode placement, recordings were carried out for 15 min, including 5 min for the stabilization of ECG.

For transthoracic echocardiography (TTE), transthoracic 2-D and M-mode images were obtained with a Visualsonics high resolution VEVO2100 system (VisualSonics, Toronto, Canada) with a 20-MHz transducer. Images were captured on cine loops at the time of the study and measurements were subsequently obtained off-line. Images were obtained from parasternal long-and short-axis views. The M-mode derived anteroposterior left atrial (LA) end diastolic diameter was measured from the parasternal long-axis according to American Society of Echocardiography procedures[4]. M-mode in short axis view was used to measure the thickness of the interventricular septum (IVS) and left ventricular posterior wall, as well as left ventricular internal diameter. All M-mode measurements were performed in end-diastole and end-systole according to the leading-edge method. The left ventricle (LV) structural parameters measured from short axis view in M-mode were used in the calculation of LV ejection fraction (EF) and LV fractional shortening (FS). All measurements were

performed excluding the respiratory peaks and obtained in triplicate; the mean value was used for data analysis. All calculated parameters were automatically computed by the VEVO2100 standard measurement package.

4. Western blots

Rat heart samples for protein analysis were fresh frozen in liquid nitrogen, weighed on an electronic balance and stored in liquid nitrogen until transfer into a -80°C freezer. All samples were stored in a -80°C freezer until used. Rat samples for histological analysis were fixed in formaldehyde at room temperature and embedded in paraffin blocks. For western blots, samples of the atria were lysed in complete RIPA buffer (10 mM Tris-HCl pH 7.4, 150mM NaCl, 1% NP40, 0.1% sodium dodecyl sulfate (SDS), 1mM phenylmethylsulfonyl fluoride (PMSF), 1x PhosStop and 1x protease inhibitor cocktail (Roche)) and homogenized by Sonic Dismemebrator 100 (Fisher Scientific). The protein concentration of tissue homogenates was measured using Bio-Rad Protein Assay, and equal amounts of soluble protein were separated on 12% polyacrylamide gels, transferred onto nitrocellulose membrane, and followed by routine western blot analysis. The sources of the primary antibodies are listed in Supplementary Table 2. HRP conjugated secondary antibodies were from BioRad Laboratories or Sigma.

5.Quantitative Real-time PCR

For quantitative real-time PCR, total RNA from rat atria was extracted using Trizol reagent (Invitrogen), and 2 μg of total RNA was used for reverse transcription reaction using Reverse Transcription & cDNA Synthesis Kit-Advantage RT for PCR Kit (Clontech Laboratories) followed by quantitative PCR using FastStart Universal SYBR Green Master (Rox) (Roche Applied Science). The primers employed were as follows: MYL4: sense 5' AAA CCC AAG CCT GAA GAG ATG 3'. antisense 5' CAG TGC TCC GTA ACA ACC ACC 3'. glyceraldehyde 3-phosphate dehydrogenase (GAPDH): sense 5' ACT CCC TCA AGA TTG TCA GCA 3', antisense 5' CAT ACC AGG AAA TGA GCT TCA C 3'. Results were normalized to GAPDH. The relative amount of each gene in each sample was estimated by the ΔΔCT method.

6. Histological analysis

For histological staining, sections of 5 μm thickness were sliced. Left atria and left ventricle fibrosis was obtained using Modified Masson's Trichrome Stain Kit from Scy Tek laboratories. FITC-conjugated wheat germ agglutinin (AF488, Invitrogen) was used to evaluate myocyte size. For mean myocyte size, the cross sectional area of at least 150-200 cells/sample and 4-5 samples/group were averaged. For relative left atria and left ventricle fibrosis, 6-10 fields/samples, and 4-5 samples/group were averaged. Apoptotic cells were evaluated by TUNEL staining using the In Situ Cell Death Detection Kit (Roche) following the manufacturer's instructions. Data was quantified in 3000 nuclei from 10 random fields per heart. The summarized results were expressed as TUNEL positive nuclei per 1000 nuclei. Further α-actin and TUNEL confocal staining was conducted to identify whether the apoptotic cells were cardiomyocytes. Immunostaining with PCNA was conducted to identify heart cell proliferation. The sources of the primary antibodies are listed in Supplementary Table 2. Values represented the mean of three independent experiments.

7. Construction of plasmids carrying MYL4 wild type (WT) and mutant sequences and purification of their expressed proteins

Synthetic WT and mutant DNA full sequences were cloned into the BamHI and EcoRI sites of the pcDNA3.1+ to pcDNA3.1-*MYL4*-GG (the WT), pcDNA3.1-*MYL4*-AA (the *E11K*) and pcDNA3.1-*MYL4*-12bp del (the *Del,* which deleted 4 consecutive amino acids near to the *MYL4 p.E11* site) recombinant plasmid, and then confirmed by sequencing. Plasmids were transformed into *DH5α* cells and transformants were selected on ampicillin (125 mg/L) containing agar plates. Protein expression and purification was accomplished by Sangon Biotech Co., Ltd (Shanghai, China).

8. Assays of ATPase activities with the mutant and WT essential myosin light chain

ATPase activities were determined by measuring inorganic phosphate release using the enzyme linked inorganic phosphate assay (ELIPA, Cytoskeleton, Cat. # BK051) according to the manufacturers' instructions. The reactions were conducted in a 96 well plate format (200 μl reaction volumes). Each reaction contains 0.2 mM MESG, 0.3 U PNP, 15 μM taxol, 15 mM PIPES pH 7.0, 5 mM MgCl2, 0.7 mM ATP, 15 ng/ml F-actin (Cytoskeleton, Cat. # AKF99) and 3 ng/ml myosin motor protein (Cytoskeleton, Cat. # MY02) (or 1.5 ng /ml

HMM or 0.75 ng /ml S1). Mutant or wild-type *MYL4* protein was added with different concentration (10, 50, 100, 500 nM). The reaction minus enzyme will serve as a background control. Reactions were measured in a Synergy™ 2 Multi-Detection Microplate Reader (BioTek Instruments, USA) set in kinetic mode at 360 nm absorbance wavelength. Readings were taken at room temperature once every 30 s for a total reaction time of 60 min.

A double-reciprocal plot of enzyme kinetics was used to determine the Km and Vmax by incubating the enzyme with varying concentrations of substrate (0.1, 0.2, 0.3, 0.4, 0.6, 0.8, 1.0, 1.2, 1.6 mM ATP was used in this study); the results are plotted as a graph of rate of reaction (v) against concentration of substrate ([S]). Vmax represents the maximum rate of reaction when the enzyme is saturated with substrate. The relationship between rate of reaction and concentration of substrate depends on the affinity of the enzyme for its substrate. This is usually expressed as the Km (Michaelis constant) of the enzyme, an inverse measure of affinity. For practical purposes, Km is the concentration of substrate which permits the enzyme to achieve half Vmax. An enzyme with a high Km has a low affinity for its substrate, and requires a greater concentration of substrate to achieve Vmax. A double-reciprocal plot of enzyme kinetics was used to determine the Km and Vmax by incubating the enzyme with different concentrations of substrate; the rates of reaction (v) against concentration of substrates ([S]) were shown by scatter plots. The relationship was modeled by the Michaelis-Menten equation: $\mathbf{v = Vmax / (1 + (Km / [S]))}$ and the Lineweaver–Burk equation of enzyme kinetics, $\mathbf{1/v=1/Vmax + Km/Vmax \times 1/[S]}$. Plotting 1/v against 1/[S] give a straight line: intercept = 1/Vmax， gradient = Km/Vmax, x intercept = -1/Km.

9. Construction of MYL4 recombinant adenoviruses and infection to the neonatal rat cardiomyocytes

The packaging, amplification, and purification of the recombinant adenovirus were accomplished by Shanghai GeneChem Co., Ltd (Shanghai, China). Briefly, recombinant plasmids were transfected into 293 cells to obtain adenovirus prestocks. Virus was purified by double cesium chloride gradient ultracentrifugation. Viral titer was determined by plaque assay and expressed as plaque forming units (pfu). The titers of stocks measured by plaque assays were $1\text{-}3\times10^{10}$ pfu/mL, with a particle/pfu ratio of 30/1. Recombinant adenoviruses were tested for the absence of wild type virus by polymerase chain reaction of the early transcriptional unit E1 and E1a. Purified virus aliquots were stored at -80°C. After two days' plating, cardiomyocytes were infected with the virus at MOI 300. The adenoviral infection experiments were carried out according to the manufacturer's instruction. The flag-tagged adenoviral vector (Ad-Flag) without expressing MYL4 was employed as the negative control.

10. Neonatal rat cardiomyocyte (NRCM) culture

The animals were handled in accordance with animal experimental protocols approved by the Animal Care and Use Committee of Shanghai Tenth Hospital. Cardiac myocytes were isolated from 1-3 day-old Sprague-Dawley rats and cultured with a modification of the method of Harary and Farley[5]. Briefly, hearts from neonatal rats were rapidly excised and washed to remove blood and debris. Then only the ventricles were carefully minced and dissociated into single cells by proteolytic enzymes (0.25% trypsin and 0.1% collagenase) during repeated digestions (5-8 times) with gentle stirring. Any contaminant fibroblasts were removed with a 1.5 hour pre-plating step. Cells were then cultured in high glucose (25%) Dulbecco's modified Eagle's medium (DMEM, Gibco, NY, USA) supplemented with 0.1 mM bromodeoxyuridine (Brdu), 15% fetal bovine serum (FBS) (Gibco, NY, USA) and 1% penicillin/streptomycin. Cells were incubated in 5% CO_2 at 37°C. Cells were characterized as cardiac myocytes by morphology and the presence of rhythmic contraction.

11. Immunofluorescence analysis

NRCM were seeded at a subconfluent density on sterile cover slips in 6-well plates and treated as indicated, then fixed with 4% paraformaldehyde in PBS for 20 min and washed three times with PBS. Cells were permeabilized with 0.5% Triton X-100 in PBS for 15 min and blocked with 5% BSA in PBS for 60 min at room temperature. Thereafter, a solution of specific primary antibody was flooded over the cells for 1 hour at 37° C. The sources of the primary antibodies were listed in Table S2. After washing with PBS, the cells were further incubated with relevant secondary antibody for 1 h at room temperature, washed with PBS, then stained with Hoechst 33342 solution (5 μg/ml diluted in PBS) for 10 min at room temperature. Fluorescence images were obtained using the DMI6000 fluorescent microscope (Leica, Germany).

12. Measurement of contractile force

Force production in atrial muscle was evaluated in vitro with direct muscle stimulation in a myocardial superfusion system (BS1501, Taimeng Co, Chengdu, China). To maintain tissue moisture, oxygenated Krebs-Henseleit buffer (35°C, with 95% O2 and 5% CO2) was continuously supplied to the atrial muscle preparation and throughout the contractile experiment. One end of the atrial muscle was fixed and the other end was connected to the tension converter through a thin wire. After the atrial muscle was fixed, 10 mV stimuli were given through an electrode. Contractile force signals were output with muscle tension

converter (FT-100, Taimeng Co, Chengdu, China. Ratio of atrial muscle contractile force to atrial muscle weight was used for statistical analysis.

Supplemental Results

1. Detailed information about each affected patient's disease history

The proband (I-7 and two relatives (II-1 and II-3 were diagnosed as displaying the complete atrial standstill (AS phenotype. The proband (I-7 showed asymptomatic sinus bradycardia on an ECG in her early twenties and often felt palpitations and had reduced exercise tolerance in her early thirties. She visited our hospital for bradycardia and lower extremity edema at 54 years old. Neither right nor left atrium could not be captured during invasive electrophysiological study at that time. II-1 and II-3 also developed total AS. They suffered from bradycardia at around 20 years old, and felt palpitations and had reduced exercise tolerance between 30 and 40 years of age. Although both II-1 and II-3 were implanted with dual chamber pacemakers to treat their bradycardia, when they came to our attention their atria could not be captured by atrial pacing.

II-19, II-21 and III-10 were diagnosed as having partial AS. III-10, aged 14, had "normal" ECG and no symptoms of palpitations or syncope. Although P waves were found in the surface ECG of these patients, there was no evident atrial mechanical activity (A waves on echocardiography. II-21, also without symptoms, had a history of atrial flutter with advanced atrioventricular block, and sinus rhythm combined with frequent atrial premature beats at age 27. II-19 had a history of syncope at her early twenties, and atrial fibrillation with junctional escape rhythm and sinus arrests. The amplitude of her P waves was very small at 36 years old.

Detailed ECG and transthoracic echocardiography (TTE) data are provided in Fig. S1, Table S1 and S3 respectively.

2. MYL4 mutation did not affect the growth of rats

There was no difference in growth or heart parameters among genotypes for both male and

female rats (Fig. S2A). *MYL4 p.E11K* also had no detectable effect on left ventricular weight, left atrial weight, right ventricular weight, right atrial weight, lung weight, liver weight, spleen weight, kidney weight and their ratios to body weight (Fig. S2).

3. Atrial contractile force in *MYL4 KO* rats

To investigate the effect of MYL4 on myocardial contraction, we measured contractile force directly by isolating and superfusing auricular appendages from *MYL4 WT* and *KO* rats (3 months old) and recording the contractile force generated in response to electrical stimulation (10 mV). The results showed that atrial muscle from the heterozygotes rats produced average of 0.39±0.21 g of tension per gram of muscle, similar to WT(0.42±0.05 g). However, the homozygous *KO* rats lost almost all contractile force generation (Fig. S7).

4. MYL4 knockdown in cultured myocytes leads to a similar myocyte death phenotype

To confirm the effect of acute MYL4 depletion, we have initiated studies to knock down MYL4 with the use of siRNA (siMYL4: 5'-GCA CCU AUG AGG ACU UCG UTT-3'; Negative control: 5'-UUC UCC GAA CGU GUC ACG UTT-3') in cultured myocytes, with the preliminary results showing that MYL4 knockdown in cultured myocytes leads to a similar myocyte death phenotype to MYL4E11K overexpression (Fig. S8).

Supplemental References:

1. Li, H., and Durbin, R. 2009. Fast and accurate short read alignment with Burrows-Wheeler transform. *Bioinformatics* 25:1754-1760.
2. DePristo, M.A., Banks, E., Poplin, R., Garimella, K.V., Maguire, J.R., Hartl, C., Philippakis, A.A., del Angel, G., Rivas, M.A., Hanna, M., et al. 2011. A framework for variation discovery and genotyping using next-generation DNA sequencing data. *Nat Genet* 43:491-498.
3. Li, M.X., Kwan, J.S., Bao, S.Y., Yang, W., Ho, S.L., Song, Y.Q., and Sham, P.C. 2013. Predicting mendelian disease-causing non-synonymous single nucleotide variants in exome sequencing studies. *PLoS Genet* 9:e1003143.
4. Lang, R.M., Bierig, M., Devereux, R.B., Flachskampf, F.A., Foster, E., Pellikka, P.A., Picard, M.H., Roman, M.J., Seward, J., Shanewise, J.S., et al. 2005. Recommendations for chamber quantification: a report from the American Society of Echocardiography's Guidelines and Standards Committee and the Chamber Quantification Writing Group, developed in conjunction with the European Association of Echocardiography, a branch of the European Society of Cardiology. *J Am Soc Echocardiogr* 18:1440-1463.
5. Harary, I., and Farley, B. 1963. In vitro studies on single beating rat heart cells. I. Growth and organization. *Exp Cell Res* 29:451-465.

Table S1. Transthoracic echocardiographic parameters in six patients

Patients	Age (year)	Left atrial diameter （mm）	Right atrial diameter （mm）	Left ventricular end diastolic diameter (mm)	Right ventricular end diastolic diameter (mm)	Inter-ventricular septal thickness (mm)	Ejection fraction (%)	Atrial septal detect
Ⅰ7	55	47	64	52	31	8	61	No
Ⅱ1	52	54	58	60	30	10	46	No
Ⅱ3	49	47	53	56	30	10	52	No
Ⅱ19	40	37	40	50	32	9	67	No
Ⅱ21	26	38	36	50	34	7	60	No
Ⅲ10	15	35	36	46	30	10	77	No

Table S2. Sources of primary antibodies

Protein	Name of the Company	Catalog number
MYL4 (for WB)	Abcam	ab180255
MYL4 (for immunofluorescence)	Santa Cruz	sc-109581
Bax	Cell Signaling	2772
caspase3	Cell Signaling	9662
BCL-2	BOSTER	BA0412
Smad2/3	Cell Signaling	8685
Phospho-Smad2/3	Cell Signaling	8828
SAPK JNK	Cell Signaling	9258
Phospho- SAPK JNK	Cell Signaling	4671
GAPDH	Santa Cruz	sc-32233
Vinculin	Santa Cruz	sc-73614
α-actin	Sigma	A2172
PCNA	Santa Cruz	Sc-56

Table S3. ECG parameters of affected patients

Patients	Age (year)	Rhythm of the heart	Atrial rate (bpm)	Ventricular rate (bpm)	PR interval (s)	QRS Time (s)	QT interval (s)
I7	47	atrial flutter with junctional escape rhythm	300	42	/*	0.08	0.44
	52	atrial flutter with junctional escape rhythm	300	44	/	0.12	0.40
	53	atrial fibrillation with junctional escape rhythm	/*	39	/	0.12	0.52
	54	atrial standstill with junctional escape	/	35	/	0.12	0.52
	55	pacemaker rhythm	/	60	/	/	0.44
II1	50	atrial standstill with junctional escape	/	40	/	0.12	0.52
	51	ECG without P wave	/	-	/	0.14	0.52
	52	pacemaker rhythm	/	60	/	0.16	0.44
II3	32	sinus bradycardia with type I AVB	47	47	0.32	0.08	0.48
	32	atrial fibrillation with junctional escape rhythm	/	38	/	0.08	0.44
	43	atrial standstill with junctional escape	/	55	/	-	-
	45	pacemaker rhythm	/	60	/	0.12	0.44
	49	pacemaker rhythm	/	60	/	0.14	0.44
II19	37	atrial flutter	300	42	/	0.10	0.48
	40	sinus rhythm with very low amplitude P waves	63	63	0.24	0.10	0.38
	40	sinus arrest	/	47	/	0.10	0.38
II21	17	atrial fibrillation with advanced atrioventricular block	/	38	/	0.08	0.38
	20	atrial flutter with periodic advanced atrioventricular block	250	75	/	0.08	0.48
	26	sinus rhythm with frequent atrial premature beats	88	88	0.18	0.10	0.36
III10	15	normal ECG	102	102	0.12	0.08	0.32

*/ represents could not be determined or not relevant.

Table S4. Candidate genes and mutations identified by preliminary bioinformatic analysis

Chromosome	Start Position	Reference Alternative Allele	Gene Symbol	Gene Feature	MaxDBAltAF	Prob.	Shared Pathway
1	3614193	C/T	*TP73*	missense	NaN	0.782373	MEISSNER_NPC_HCP_WITH_H3K4ME2_AND_H3K27ME3#349:(TP73,SCN5A) ; MIKKELSEN_NPC_HCP_WITH_H3K27ME3#341:(TP73,SCN5A)
7	123119864	G/A	*WASL*	missense	0.000279	0.692504	REACTOME_DEVELOPMENTAL_BIOLOGY#396:(WASL,SCN5A) ; REACTOME_AXON_GUIDANCE#251:(WASL,SCN5A)
9	12684066	G/A	*TYRP1*	missense	0.001952	0.685345	
1	153433892	C/T	*THBS3*	missense	0.000186	0.524582	
2	31337226	G/T	*EHD3*	missense	NaN	0.416091	
20	55573013	C/T	*PCK1*	missense	NaN	0.263967	REACTOME_DEVELOPMENTAL_BIOLOGY#396:(PCK1,SCN5A)
16	16191692	G/A	*ABCC6*	missense	NaN	0.23587	
20	23013662	C/G	*CD93*	missense	NaN	0.225944	
6	46243538	C/T	*ENPP5*	missense	0.0009	0.217383	
3	194684434	C/A	*ATP13A4*	missense	NaN	0.211032	
15	99411136	G/C	*LRRK1*	missense	NaN	0.2095	
2	55951519	C/T	*EFEMP1*	missense	0.0014	0.207807	LINDGREN_BLADDER_CANCER_CLUSTER_2B#392:(EFEMP1,GJA5) ; KAAB_HEART_ATRIUM_VS_VENTRICLE_UP#249:(EFEMP1,GJA5)
15	50400922	A/C	*MYO5A*	missense	0	0.197927	LINDGREN_BLADDER_CANCER_CLUSTER_2B#392:(MYO5A,GJA5)
10	42601019	T/C	*BMS1*	missense	0.0009	0.180562	
21	42402818	A/C	*UMODL1*	missense	0	0.179947	
3	158461775	G/A	*VEPH1*	missense	0.0005	0.158828	
17	60586853	C/A	*RGS9*	stopgain	0	0.155492	
4	2145526	A/G	*POLN*	missense	NaN	0.141428	
3	198907180	C/T	*KIAA0226*	missense	NaN	0.137165	
9	134192991	T/C	*SETX*	missense	0	0.132518	
7	150476928	C/T	*GBX1*	missense	NaN	0.116493	MEISSNER_NPC_HCP_WITH_H3K4ME2_AND_H3K27ME3#349:(GBX1,SCN5A)
2	73489360	C/T	*ALMS1*	stopgain	0.0005	0.109707	
6	43125300	G/A	*CUL7*	stopgain	NaN	0.104343	

11	117879936	C/T	*MLL*	missense	NaN	0.098939	
4	158277180	A/T	*GLRB*	missense	NaN	0.097504	
3	145174177	C/A	*C3orf58*	missense	NaN	0.08729	
15	40439348	G/A	*CAPN3*	missense	NaN	0.085638	
13	38161128	C/A	*FREM2*	missense	0.0009	0.083774	
3	195854757	G/A	*LSG1*	missense	0.0018	0.079114	
11	75933102	T/G	*C11orf30*	missense	0.0023	0.077267	
10	29011062	T/C	*BAMBI*	missense	NaN	0.074731	KAAB_HEART_ATRIUM_VS_VENTRICLE_UP#249:(BAMBI,GJA5)
1	116952209	C/A	*IGSF3*	missense	0	0.068039	
12	130804885	G/A	*SFSWAP*	missense	0.0027	0.067547	
19	12737804	C/G	*HOOK2*	missense	NaN	0.067351	
11	116136679	A/T	*BUD13*	missense	0.0005	0.06519	
16	28525058	T/A	*SULT1A1*	missense	NaN	0.063724	
2	119952880	A/C	*SCTR*	missense	NaN	0.063341	
12	121851800	C/T	*CCDC62*	missense	0.0009	0.063162	
7	44007150	A/C	*SPDYE1*	missense	NaN	0.061378	
1	103921679	T/G	*AMY2B*	missense	0.0005	0.061262	
18	70171950	C/T	*C18orf63*	missense	NaN	0.06119	
4	187865335	G/A	*FAT1*	missense	0.001667	0.060349	
15	39924544	C/T	*JMJD7-PLA2G4B*	missense	NaN	0.060081	LINDGREN_BLADDER_CANCER_CLUSTER_2B#392:(JMJD7-PLA2G4B,GJA5)
12	117001639	C/T	*VSIG10*	missense	0.0014	0.059141	
2	86125937	T/G	*POLR1A*	missense	0	0.058237	
10	45119203	C/T	*OR13A1*	missense	0.0005	0.057929	
20	33553765	G/C	*CEP250*	missense	0	0.057153	
2	105290697	G/A	*TGFBRAP1*	missense	0.0009	0.056554	
14	46574027	T/G	*MDGA2*	missense	0	0.05636	
14	93770729	G/A	*PPP4R4*	missense	NaN	0.055602	
4	3078914	C/T	*HTT*	missense	0	0.055428	
11	117479160	G/A	*TMPRSS4*	missense	NaN	0.051357	RODWELL_AGING_KIDNEY_NO_BLOOD_UP#222:(TMPRSS4,SCN5A)
11	85123317	T/A	*SYTL2*	missense	0.000465	0.045785	RODWELL_AGING_KIDNEY_NO_BLOOD_UP#222:(SYTL2,SCN5A)
20	42476573	G/A	*HNF4A*	missense	0.0018	0.053836	REACTOME_DEVELOPMENTAL_BIOLOGY#396:(HNF4A,SCN5A)

8	11339102	C/G	*FAM167A*	missense	NaN	0.055123	MIKKELSEN_NPC_HCP_WITH_H3K27ME3#341:(FAM167A,SCN5A)
20	36980550	G/A	*PPP1R16B*	missense	NaN	0.03704	LINDGREN_BLADDER_CANCER_CLUSTER_2B#392:(PPP1R16B,GJA5)
6	132686909	G/T	*MOXD1*	missense	NaN	0.029112	LINDGREN_BLADDER_CANCER_CLUSTER_2B#392:(MOXD1,GJA5) ; RODWELL_AGING_KIDNEY_NO_BLOOD_UP#222:(MOXD1,SCN5A)
17	42641818	G/A	*MYL4*	missense	NaN	0.037877	KAAB_HEART_ATRIUM_VS_VENTRICLE_UP#249:(MYL4,GJA5)
17	38071023	G/C	*TUBG2*	missense	NaN	NaN	
12	12123659	A/C	*BCL2L14*	missense	NaN	0.048043	COULOUARN_TEMPORAL_TGFB1_SIGNATURE_UP#109:(BCL2L14,GJA5)
4	74525277	A/T	*AFP*	missense	NaN	0.04082	COULOUARN_TEMPORAL_TGFB1_SIGNATURE_UP#109:(AFP,GJA5)

Table S5. The top 10 gene list based on GeneWanderer

Rank	Gene Symbol	Score
1	CRHR1	0.0783
2	MYL4	0.05867
3	CNTNAP1	0.05712
4	FZD2	0.05316
5	HSD17B1	0.03438
6	STAT3	0.02984
7	GFAP	0.02658
8	MPP3	0.02526
9	PSMD3	0.02502
10	PLCD3	0.0213

Table S6. The top 10 gene list based on Endeavour

Rank	Global prioritization	Annotation EnsemblEst	Annotation GeneOntology	Annotation Interpro	Annotation Kegg	Annotation Swissprot	Blast	CisRegModule	Expression SonEtAl	Expression SuEtAl	Interaction Bind	Interaction BioGrid	Interaction Hprd	Interaction InNetDb	Interaction Intact	Interaction Mint	Interaction String	Motif	Precalculated Ouzounis	Precalculated Prospectr	Text
1	GJC1	SNX11	GAST	GJC1	GJC1	GJC1	GJC1	UBE2Z	MYL4	HSD17B1	HSD17B1	HSD17B1	MPP2	MYL4	MYL4	MYL4	GJC1	HSD17B1	STAT3	HCRT	GJC1
2	MYL4	KRT16	KCNH4	GAST	CCR7	HOXB7	MAPT	HOXB2	MEOX1	C17orf53	C17orf53	C17orf53	FZD2	KRT37	KRT13	KRT13	MPP2	GJC1	THRA	ATP6V0A1	MAPT
3	MPP3	TMEM101	CCR7	KCNH4	CRHR1	KCNH4	CASC3	KRTAP3-2	SNF8	HOXB1	HOXB1	HOXB1	ACLY	MPP2	KRT16	KRT16	KCNH4	HOXB4	HOXB13	KRT10	HOXB6
4	MAPT	MYL4	CCR10	CCR7	CNTNAP1	JUP	ASB16	KRT33A	RAMP2	KRT9	KRT9	KRT9	GFAP	ATP5G1	KRT14	KRT14	ORMDL3	IGF2BP1	HCRT	ITGB3	HOXB7
5	GFAP	ITGB3	CRHR1	CCR10	FZD2	BECN1	KRT10	GFAP	HOXB6	NAGLU	NAGLU	NAGLU	STAT5B	HAP1	KRT10	KRT10	EZH1	SLC4A1	KRT36	CCR7	GNGT2
6	KCNH4	MLX	MPP3	CRHR1	AOC3	GNGT2	KRTAP4-3	CDC6	GRN	HOXB5	HOXB5	HOXB5	MAPT	ATP6V0A1	GFAP	GFAP	RAB5C	PTRF	ITGB3	ITGA2B	HOXB5
7	WNK4	CNTD1	CNTNAP1	MPP3	KRT19	CNP	KRTAP3-1	KRT25	DHX8	PNPO	PNPO	PNPO	STAT5A	JUP	KRT9	KRT9	MYL4	LRRC37A|LRRC37A2	G6PC	WNT9B	HOXB4
8	MPP2	TBX21	FZD2	CNTNAP1	GCN5L2	RND2	DUSP3	C17orf53	ATP5G1	ATP5G1	ATP5G1	ATP5G1	HSD17B1	KRT19	KRT37	KRT37	WNK4	HOXB8	BRCA1	FKBP10	HOXB1
9	ATP6V0A1	B4GALNT2	MPP2	FZD2	RPL27	CCR7	KRT23	WNT3	NKIRAS2	MYL4	MYL4	MYL4	C17orf53	KRT17	MPP2	MPP2	MPP3	WNK4	SOST	CNTNAP1	CDK5RAP3
10	STAT3	GCN5L2	AOC3	MPP2	ACLY	FZD2	KRTAP3-3	IGF2BP1	KRT34	GAST	GAST	GAST	HOXB1	G6PC	ATP5G1	ATP5G1	SP2	NBR2	NAGLU	AOC2	KCNH4

Table S7. *MYL4* ^{E11K} knock-in rat ECG parameters.

Genotype	WT (N=9)				*MYL4* $^{E11K+/-}$ (N=15)				*MYL4* $^{E11K+/+}$ (N=10)			
age	15d	1 month	3 month	6 month	15d	1 month	3 month	6 month	15d	1 month	3 month	6 month
Heart rate (bpm)	401±19	479±9.6	422±17	330±27	384±9	436±11	402±14	364±14	357±20	440±14	416±8	344±14
P wave amplitude (mv)	0.13±0.01	0.13±0.01	0.11±0.01	0.08±0.01#	0.14±0.01	0.08±0.01 ***	0.07±0.01 **	0.07±0.01#	0.10±0.01**	0.09±0.01 ***	0.03±0.01 ***	0.01±0.01 ***#
PR interval (ms)	45.0±2.3	44.2±1.3	46.3±0.8	45.4±1.2	49.0±1.7	44.9±1.0	52.5±1.2 ***	49.3±2.0*#	51.0±2.0**	54.5±3.2 ***	56.2±1.5 ***	59±--- #
QRS duration (ms)	18.6±0.3	20.2±1.0	20.9±0.5	21.0±0.4	19.3±0.3	18.5±0.4	19.7±0.3	20.5±0.8	19.8±0.4	20.9±0.7	20.1±0.7	20.4±0.6
QT interval (ms)	59.0±1.1	60.2±1.9	65.5±2.7	67.6±3.1	64.8±1.5*	62.9±1.4	71.5±1.4	67.5±2.4#	61.2±1.7	65.1±1.8	73.6±2.8*	76.4±1.7*#
Rats with sinus rhythm/total	9/9	9/9	9/9	9/9	15/15	15/15	15/15	15/15	10/10	10/10	6/10	2/10

Data are mean ± SEM. *p<0.05; ** p<0.01; *** p<0.001 vs. WT, #p<0.05 among 15 d, 1 month, 3 month and 6 month rats.

Table S8. Measurements of *MYL4* $^{E11K+/-}$ mutation rat TTE.

Genotype	WT				*MYL4* $^{E11K+/-}$				*MYL4* $^{E11K+/+}$			
age	15d	1 month	3 month	6 month	15d	1 month	3 month	6 month	15d	1 month	3 month	6 month
N	6	4	4	4	5	6	5	6	6	5	4	5
LA (mm)	1.8±0.1	2.3±0.1	2.5±0.2	3.2±0.1	1.9±0.1	2.5±0.1	3.1±0.1*	3.8±0.1*	1.9±0.1	2.3±0.1	3.9±0.2***	4.5±0.3***
IVS-d (mm)	0.9±0.0	1.4±0.1	1.4±0.1	2.3±0.1	0.9±0.1	1.4±0.1	1.7±0.2	1.9±0.1	0.9±0.1	1.7±0.2	1.7±0.1	2.4±0.3
IVS-s (mm)	1.5±0.1	2.4±0.2	2.3±0.1	3.5±0.2	1.6±0.1	2.2±0.1	2.8±0.3	3.1±0.1	1.5±0.1	2.5±0.2	2.3±0.2	3.3±0.2
LVID-d (mm)	4.3±0.2	5.6±0.1	6.7±0.3	6.8±0.5	4.0±0.1	5.6±0.1	6.6±0.5	6.8±0.2	4.2±0.1	5.4±0.1	6.6±0.5	7.0±0.5
LVID-s (mm)	2.4±0.2	2.6±0.2	3.7±0.1	3.8±0.5	2.2±0.1	2.7±0.2	3.6±0.4	4.1±0.2	2.4±0.1	2.7±0.2	4.3±0.2	4.5±0.5
LVPW-d (mm)	0.8±0.1	1.6±0.1	1.9±0.0	2.6±0.1	1.1±0.1	1.6±0.1	2.1±0.1	2.2±0.2	1.0±0.1	1.5±0.2	2.0±0.1	2.4±0.2
LVPW-s (mm)	1.5±0.1	2.8±0.1	2.8±0.2	2.9±0.3	1.6±0.1	2.7±0.1	2.9±0.1	3.1±0.2	1.6±0.1	2.4±0.3	2.6±0.1	3.3±0.2
EF (%)	74±3.2	85±2.6	75±1.9	74±3.4	75±1.6	82±1.7	75±2.0	68±2.3	73±1.2	80±3.4	62±1.1***	65±4.5
FS (%)	43±3.0	55±2.9	45±1.9	44±2.9	44±1.4	52±1.8	45±1.8	39±1.9	42±1.0	50±3.3	35±0.8**	37±3.3

Data are presented as mean ± SEM. * p <0.05; ** p <0.01; *** p<0.001 vs. WT.

LA: Left atrial diastolic diameter; LVID-d: Left ventricular diastolic dimension; LVID-s:Left ventricular systolic dimension; LVPW-d: Posterior wall thickness diastole; LVPW-s: Posterior wall thickness systole； IVS-d: Interventricular septum thickness diastole; IVS-s: Interventricular septum thickness systole; EF: Left ventricular ejection fraction; FS: Left ventricular fractional shortening.

Table S9. *MYL4 KO* rat ECG measurements.

Genotype	WT			*MYL4 HT*			*MYL4 KO*		
age	1 month	3 month	⩾6 month	1 month	3 month	⩾6 month	1 month	3 month	⩾6 month
N	9	9	9	12	10	9	5	4	4
Heart rate (bpm)	479±10	422±17	402±18#	459±6	405±18	346±21*#	465±8	433±32	319±18*#
P wave amplitude (mv)	0.13±0.01	0.11±0.01	0.07±0.00#	0.11±0.01**	0.09±0.01*	0.06±0.01#	0.04±0.02***	------	------
PR interval (ms)	44.2±1.2	46.3±0.8	48.4±1.3	50.8±1.4**	48.4±1.5*	54.7±1.0*#	59.0±1.0***	------	------
QRS duration (ms)	20.2±1.0	20.6±0.5	21.6±0.4	19.9±0.6	19.9±0.5	21.0±0.7	22.8±1.2	25.0±1.4*	26.0±1.0*
QT interval (ms)	65.6±1.9	65.5±2.7	66.4±4.0	62.4±1.0	70.7±1.3	76.2±6.3#	75.0±2.8***	85.0±1.1***	113.1±7.1***#
Rats with sinus rhythm/total	9/9	9/9	9/9	12/12	9/10	9/9	2/5	0/4	0/4

Data are presented as mean ± SEM. * p<0.05; ** p<0.01; *** p<0.001 vs. WT, # p <0.05 among 1 month, 3 month and ⩾6 month.

Table S10. *MYL4 KO* rat TTE results.

Genotype	WT	*MYL4 HT*	*MYL4 KO*
N	3	5	3
LA (mm)	5.4±0.0	5.8±0.3*	8.7±1.6**
IVS-d (mm)	2.1±0.1	2.0±0.2	1.9±0.4
IVS-s (mm)	3.5±0.1	3.2±0.2	3.0±0.2
LVID-d (mm)	8.6±0.5	8.6±0.4	10.0±2.2
LVID-s (mm)	5.3±0.2	5.1±0.3	7.5±1.7
LVPW-d (mm)	2.0±17	1.9±0.3	2.3±0.4
LVPW-s (mm)	2.6±0.0	3.3±0.1	5.3±1.5*
EF (%)	66±1.0	70±2.0	46±0.2***
FS (%)	38±1.0	41±1.7	24±0.5**

Data are presented as mean ± SEM. * $p<0.05$; ** $p<0.01$; *** $p<0.001$ vs. WT.

LA: Left atrial diastolic diameter; LVID-d: Left ventricular diastolic dimension; LVID-s:Left ventricular systolic dimension; LVPW-d: Posterior wall thickness diastole; LVPW-s: Posterior wall thickness systole； IVS-d: Interventricular septum thickness diastole; IVS-s: Interventricular septum thickness systole; EF: Left ventricular ejection fraction; FS: Left ventricular fractional shortening.

Table S11. *MYL4*^{del} rat ECG measurements.

Genotype	WT (N=4)			*MYL4*$^{del+/-}$ (N=5)			*MYL4*$^{del+/+}$ (N=4)		
age	1 month	6 month	12month	1 month	6 month	12 month	1 month	6 month	12 month
Heart rate (bpm)	485±9	426±18	387±9 #	461±7	406±29	384±8#	480±16	399±12	395±10#
P wave amplitude (mv)	0.11±0.01	0.09±0.01	0.11±0.02	0.10±0.01	0.07±0.01	0.09±0.01	0.10±0.01	0.07±0.01	0.08±0.01#
PR interval (ms)	49.5±1.3	52.3±1.1	53.8±1.3	45.2±1.0	51.0±1.7	54.5±1.5#	50.0±2.3	51.7±4.3	52.0±2.5
QRS duration (ms)	18.3±1.0	18.8±0.8	19.8±0.6	19.0±0.5	20.5±0.9	19.8±0.8	20.3±0.9	20.0±0.6	20.4±0.8
QT interval (ms)	60.8±0.9	60.8±4.2	63.5±2.8	59.2±1.7	61.3±1.9	67.7±2.7	62.8±4.7	64.3±1.7	63.0±4.0
Rats with sinus rhythm/total	4/4	4/4	4/4	5/5	5/5	5/5	4/4	4/4	4/4

Data are presented as mean ± SEM #indicated ANOVA Analysis $p<0.05$ among 1month,3month and ⩾6month.

Table S12. *MYL4*^{del} rat TTE measurements.

Genotype	WT	*MYL4*$^{del+/-}$	*MYL4*$^{del+/+}$
N	3	5	3
LA (mm)	5.2±0.2	5.0±0.1	5.2±0.2
IVS-d (mm)	3.1±0.1	2.9±0.2	3.1±0.3
IVS-s (mm)	1.8±0.1	1.9±0.1	2.0±0.1
LVID-d (mm)	7.8±0.2	7.6±0.2	7.4±0.4
LVID-s (mm)	4.1±0.2	4.5±0.2	4.1±0.2
LVPW-d (mm)	2.1±0.2	2.1±0.1	2.3±0.1
LVPW-s (mm)	3.1±0.1	3.0±0.3	3.0±0.3
EF (%)	77±2.4	71±2.5	74±1.9
FS (%)	47±2.2	42±2.0	44±1.7

Data are presented as mean ± SEM

LA: Left atrial diastolic diameter; LVID-d: Left ventricular diastolic dimension; LVID-s: Left ventricular systolic dimension; LVPW-d: Posterior wall thickness diastole; LVPW-s: Posterior wall thickness systole； IVS-d: Interventricular septum thickness diastole; IVS-s: Interventricular septum thickness systole; EF: Left ventricular ejection fraction; FS: Left ventricular fractional shortening.

Supplemental Figure Legends:

Figure S1. Clinical data of patients .

A. (Left Lead II ECG of the proband (I-7 at different ages: 47 years old, atrial flutter (indicated by arrow with junctional escape rhythm; 52 years old, atrial flutter (indicated by arrow with junctional escape rhythm; 53 years old, atrial fibrillation (irregular baseline due to fibrillation with junctional escape rhythm; 54 years old, atrial standstill with junctional escape; 56 years old, paced rhythm. (Right Invasive electrophysiological study: atria could not be stimulated, even with maximum voltage.

B. ECG of II-1: 50 years old, atrial standstill with junctional escape; 51 years old, atrial standstill with junctional escape; 52 years old, paced rhythm, no P waves following atrial pacing signal (indicated by arrow.

C. ECG of II-3: 32 years old, sinus bradycardia with I° atrial-ventricle block (AVB or atrial fibrillation with junctional escape rhythm; 43 years old, atrial standstill with junctional escape; 45 years old, and 49 years old, paced rhythm, no P waves following atrial pacing signal (indicated by arrow.

D. ECG of II-19: 37 years old, atrial flutter; 40 years old, sinus rhythm with very low amplitude P wave (indicated by arrow； 40 years old, Holter ECG at night 03:54 AM, sinus arrest (no heart beat for 2.3 seconds.

E. Clinical data of III-10: 15 years old, normal ECG; TTE lacked A spike.

F. Clinical data of II-21: 17 years old, atrial fibrillation with advanced AVB; 20 years old, Holter ECG, atrial flutter (indicated by arrow with advanced AVB; 26 years old, sinus rhythm with frequent atrial premature beats, (indicated by arrow); TTE lacked A wave.

Figure S2. *MYL4 p.E11K* did not affect rat growth or heart tissue weight.

A: There was no difference of growth among three genotypes in both male and female *MYL4 p.E11K* knock-in rats.

B-K: *MYL4 p.E11K* has no detectable effect on left ventricular weight, left atrial weight, right ventricular weight, right atrial weight, lung weight, liver weight, spleen weight, kidney

weight and their ratios to body weight.

Data are mean ± SEM.

Figure S3. *MYL4 p.E11K* exacerbated atrial cell (fibroblast) proliferation but did not affect the cell proliferation in ventricles.

Representative images and statistical data for PCNA staining of sections from WT, *MYL4 E11K*$^{+/-}$ and *MYL4 E11K*$^{+/+}$ rats (4-5 hearts per group, 6-10 fields per heart for each group.

A-B atria; C-D ventricle.

Values are mean ± SEM. * vs. WT, $p<0.05$, # $p<0.05$ among 15 d, 1 month, 3 month and 6 month rats.

Figure S4. *MYL4 E11K* does not affect the cell size of the atrial or ventricle cardiomyocytes, or NRCM.

Cell sizes were measured based on FITC-conjugated wheat germ agglutinin staining. There were no differences among WT, *MYL4 E11K*$^{+/-}$ rat and *MYL4 E11K*$^{+/+}$ rats in atrial (A-B or ventricular (C-D cardiomyocyte size.

E-F: For NRCM cell sizes were measured based on α-actin staining. There were no differences among WT, *MYL4 E11K*$^{+/-}$ and *MYL4 E11K*$^{+/+}$ over-expression groups.

Figure S5. *MYL4 E11K* does not affect ventricular fibrosis or apoptosis.

A and B: Ventricle fibrosis obtained by Masson staining averaged for 4-5 hearts per group (6-10 fields per heart for each group.

C and D: Representative images and mean data for TUNEL staining of ventricle sections from WT, *MYL4 E11K*$^{+/-}$ and *MYL4 E11K*$^{+/+}$rats.

Figure S6. *MYL4 KO* and *MYL4 del* targeting strategies and identification.

The *MYL4 KO* and *MYL4 del* rat models were constructed using CRISPR/Cas-mediated genome editing (A. The genotypes were identified by Sanger Sequencing (B-C. *MYL4 KO* was verified by Western Blot and Real-time PCR (D-F. *MYL4 E11K* also was verified by Western Blot and Real-time PCR (G-I.

Figure S7. Lost atrial contractile force in *MYL4 KO* rats.

Figure S8. MYL4 knockdown in cultured myocytes leaded to a similar myocyte death phenotype.

MYL4 was knocked down with the use of siRNA (siMYL4: 5’-GCA CCU AUG AGG ACU UCG UTT-3’; Negative control: 5’-UUC UCC GAA CGU GUC ACG UTT-3’ in cultured myocytes, caspase 3, Bax and Bcl-2 protein level were detected by WB.

Data are mean ± SEM. Protein from 3 independent samples were subjected to immunoblot for each groups. *p<0.05.

Figure S9. *MYL4 KO* or *del* mutations do not cause ventricular fibrosis.

Ventricular fibrosis measured with Masson staining was averaged for 4-5 hearts per group (6-10 fields per heart for each group.

A-B: Ventricular fibrosis for *MYL4 KO* rats.

C-D: Ventricular fibrosis for *MYL4 del* rats.

Figure S10. ATPase activity assays .

The ATPase activities were determined based on Km and Vmax of myosin. Both Km and Vmax were significantly smaller in the presence of MYL4-E11K protein than MYL4-WT protein, but MYL4-Del protein did not affect myosin ATPase activity.

HMM: Heavy Meromyosin Protein; S1: Myosin head subfragment-1 domain. Both HMM and S1 have ATPase activity.

* p<0.05.

Figure S1.

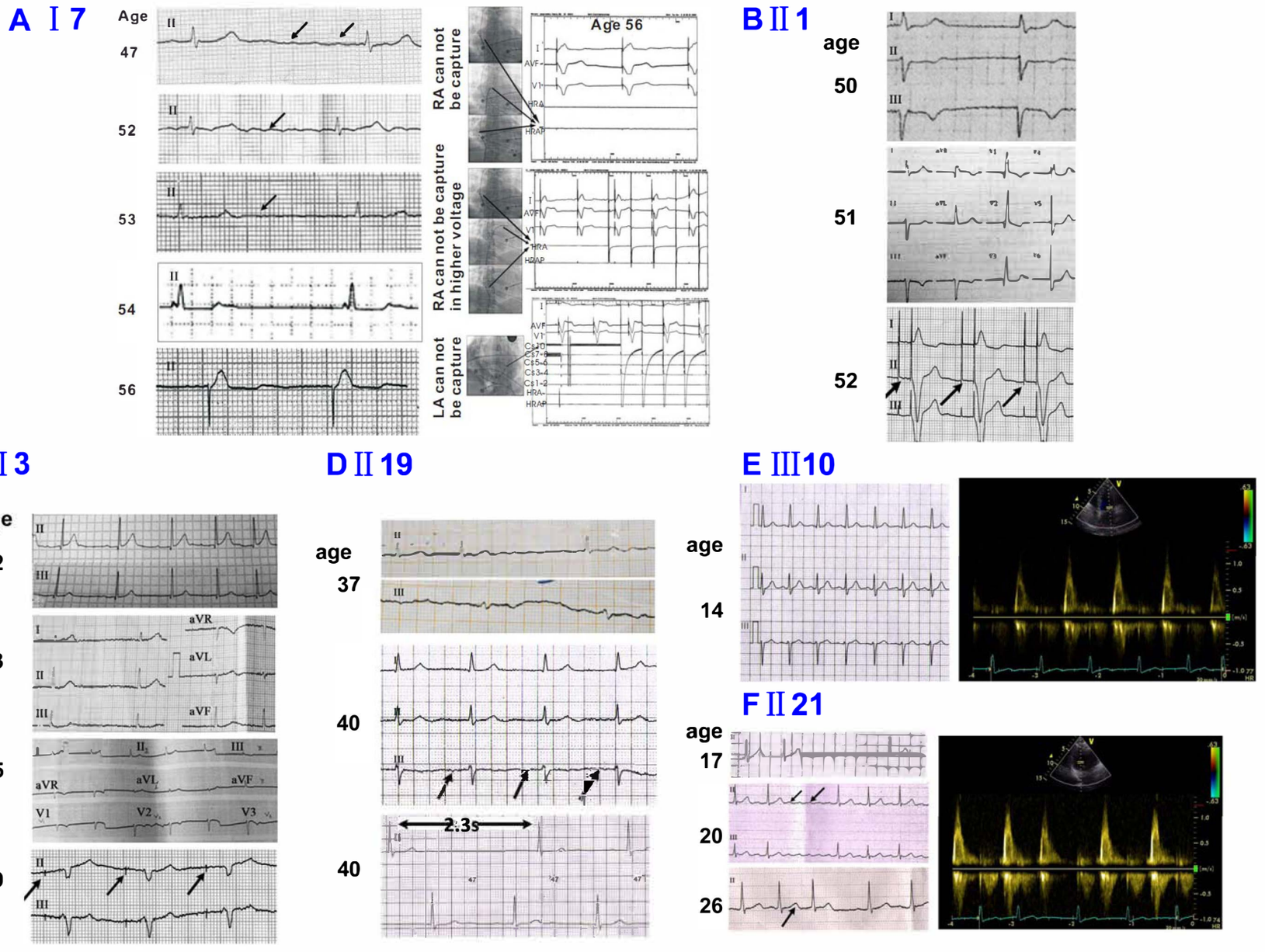

Clinical data of patients

A. (Left) Lead II ECG of the proband (I-7) at different ages: 47 years old, atrial flutter (indicated by arrow) with junctional escape rhythm; 52 years old, atrial flutter (indicated by arrow) with junctional escape rhythm; 53 years old, atrial fibrillation (irregular baseline due to fibrillation) with junctional escape rhythm; 54 years old, atrial standstill with junctional escape; 56 years old, paced rhythm. (Right) Invasive electrophysiological study: atria could not be stimulated, even with maximum voltage.

B. ECG of II-1: 50 years old, atrial standstill with junctional escape; 51 years old, atrial standstill with junctional escape; 52 years old, paced rhythm, no P waves following atrial pacing signal (indicated by arrow).

C. ECG of II-3: 32 years old, sinus bradycardia with I° atrial-ventricle block (AVB) or atrial fibrillation with junctional escape rhythm; 43 years old, atrial standstill with junctional escape; 45 years old, and 49 years old, paced rhythm, no P waves following atrial pacing signal (indicated by arrow).

D. ECG of II-19: 37 years old, atrial flutter; 40 years old, sinus rhythm with very low amplitude P wave (indicated by arrow) ; 40 years old, Holter ECG at night 03:54 AM, sinus arrest (no heart beat for 2.3 seconds).

E. Clinical data of III-10: 15 years old, normal ECG; TTE lacked A spike.

F. Clinical data of II-21: 17 years old, atrial fibrillation with advanced AVB; 20 years old, Holter ECG, atrial flutter (indicated by arrow) with advanced AVB; 26 years old, sinus rhythm with frequent atrial premature beats, (indicated by arrow); TTE lacked A wave.

Figure S2.

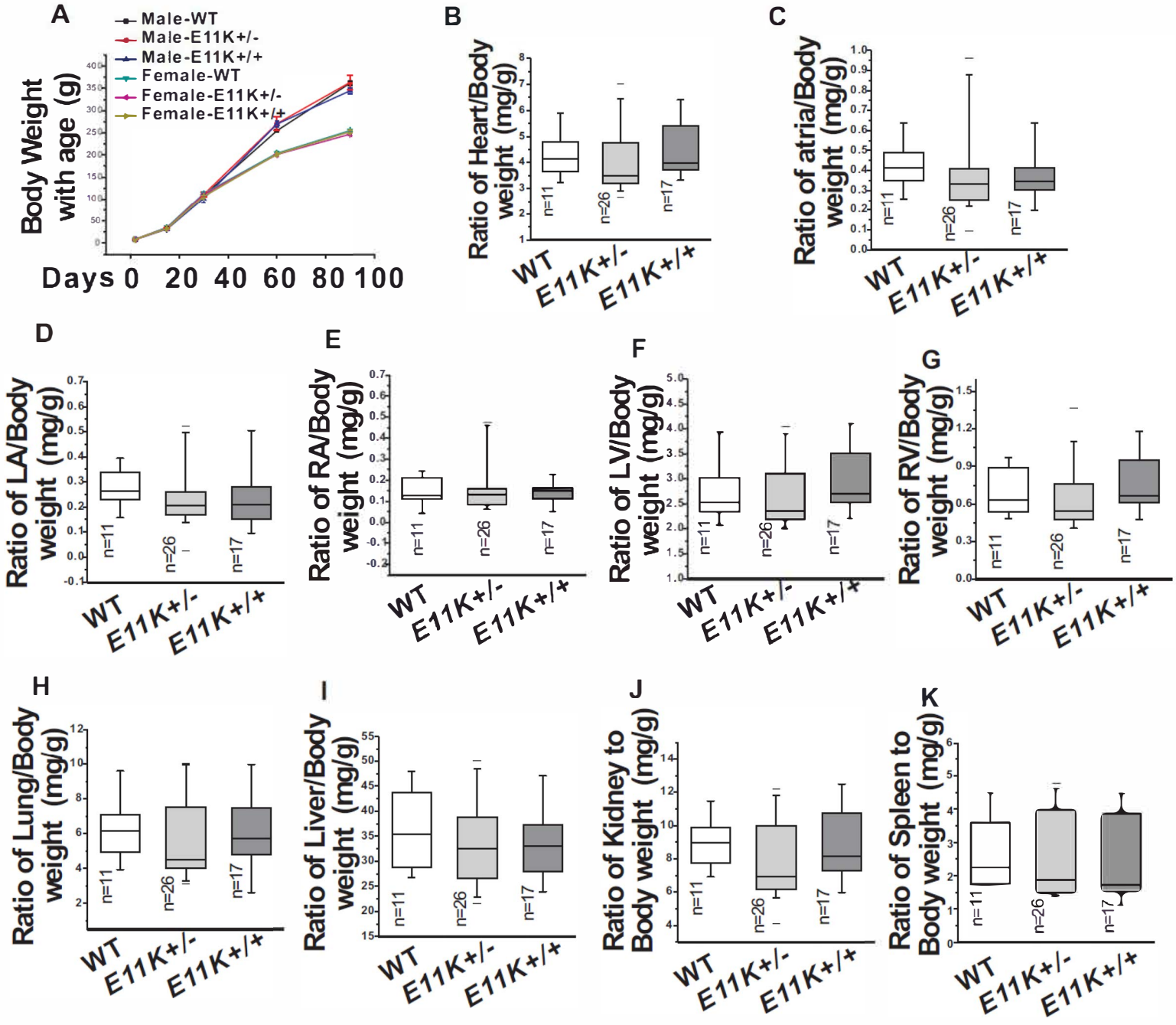

MYL4 p.E11K **did not affect rat growth or heart tissue weight.**

A: There was no difference of growth among three genotypes in both male and female *MYL4 p.E11K* knock-in rats.

B-K: *MYL4 p.E11K* has no detectable effect on left ventricular weight, left atrial weight, right ventricular weight, right atrial weight, lung weight, liver weight, spleen weight, kidney weight and their ratios to body weight.

Data are mean ± SEM.

Figure S3.

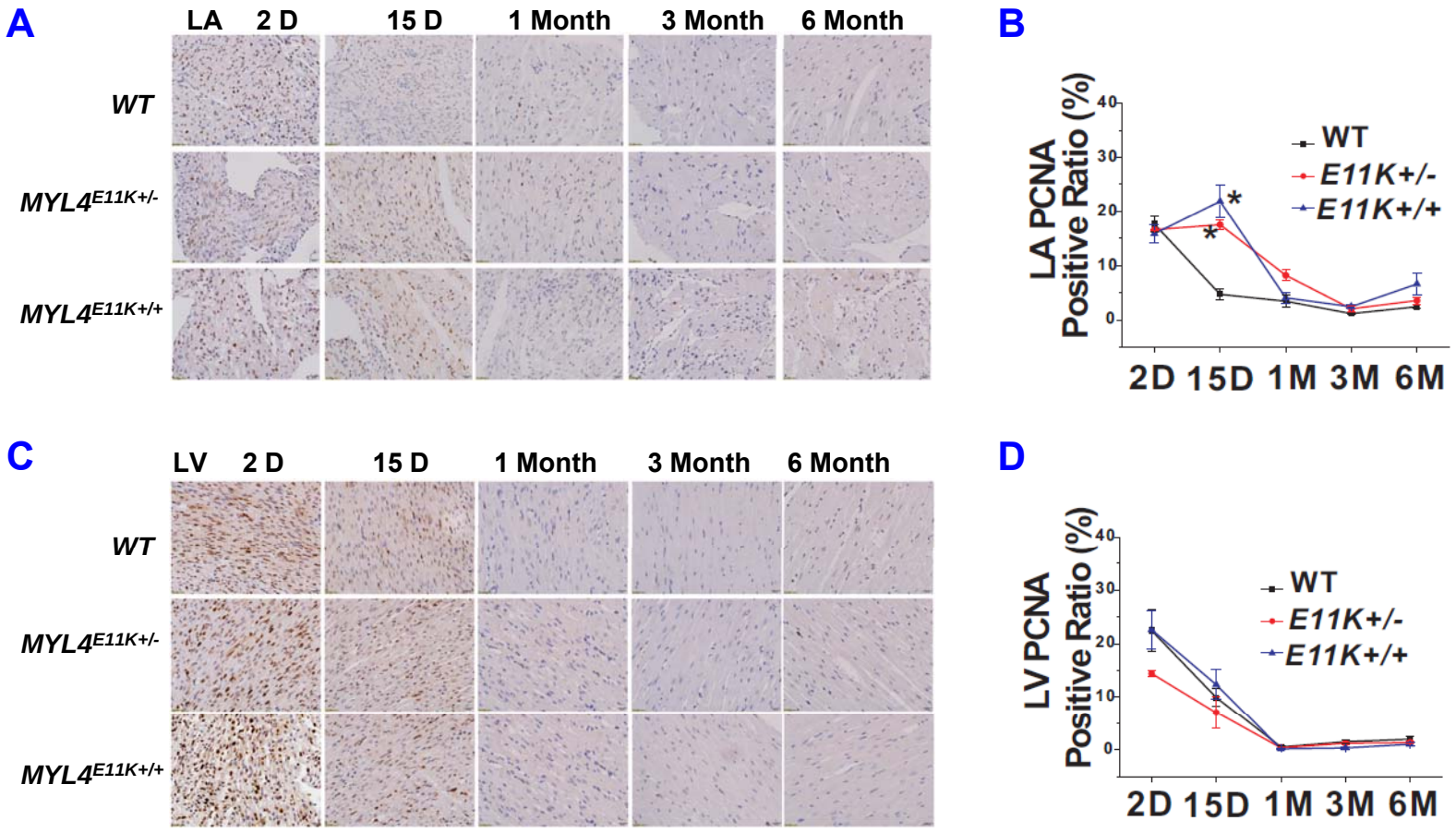

***MYL4*p.E11K exacerbated atrial cell (fibroblast) proliferation but did not affect the cell proliferation in ventricles.** Representative images and statistical data for PCNA staining of sections from WT, *MYL4 E11K*$^{+/-}$ and *MYL4 E11K*$^{+/+}$ rats (4-5 hearts per group, 6-10 fields per heart for each group).
A-B atria; C-D ventricle.
Values are mean ± SEM. * vs. WT, $p<0.05$, # $p<0.05$ among 15 d, 1 month, 3 month and 6 month rats.

Figure S4.

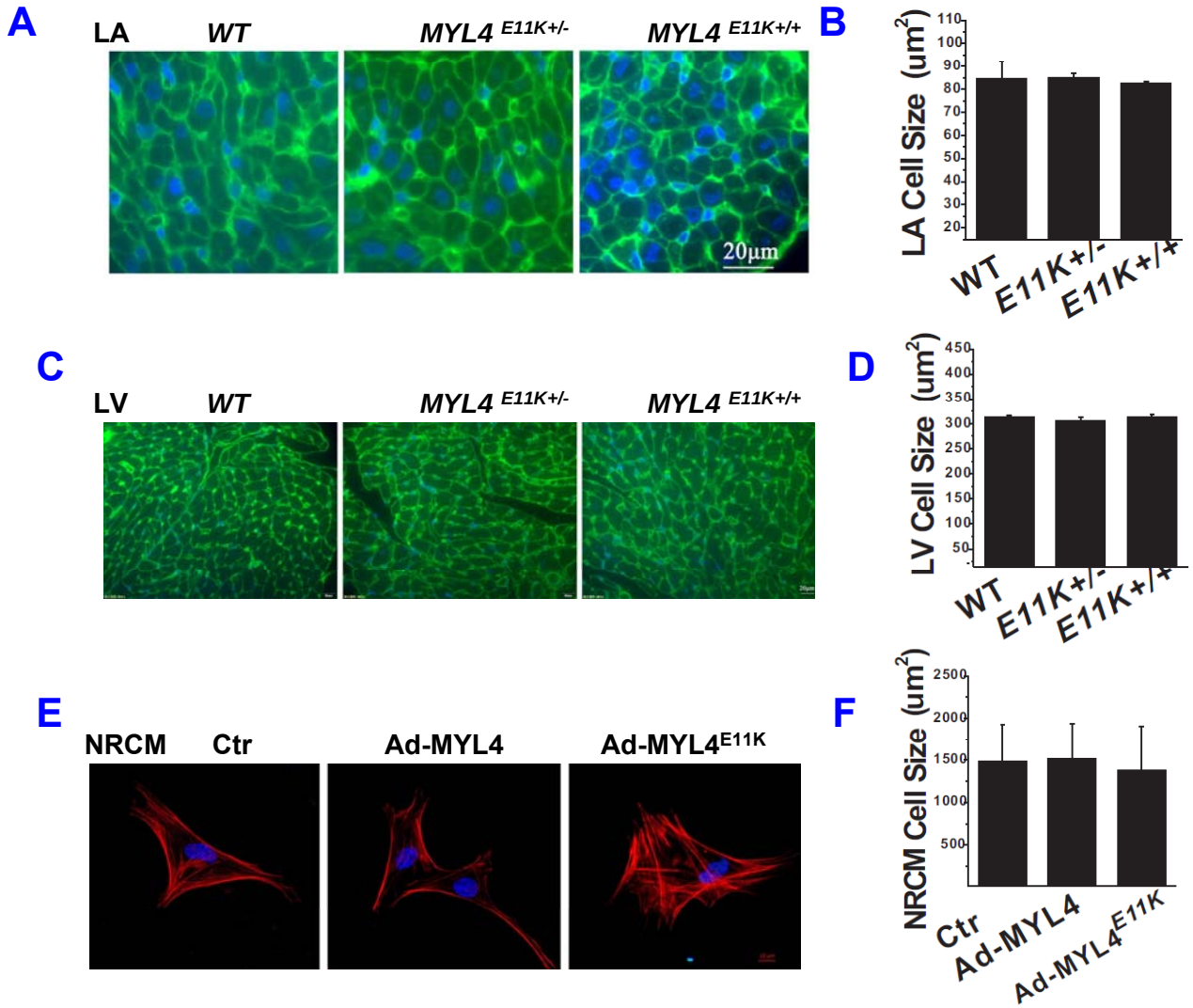

***MYL4E11K* does not affect the cell size of the atrial or ventricle cardiomyocytes, or NRCM.**

Cell sizes were measured based on FITC -conjugated wheat germ agglutinin staining. There were no differences among WT, *MYL4 E11K*$_{+/-}$rat and *MYL4 E11K*$_{+/+}$rats in atrial (A-B) or ventricular (C-D) cardiomyocyte size.

E-F: For NRCM cell sizes were measured based on α-actin staining. There were no differences among WT, *MYL4 E11K*$_{+/-}$and *MYL4 E11K*$_{+/+}$over-expression groups.

Figure S5.

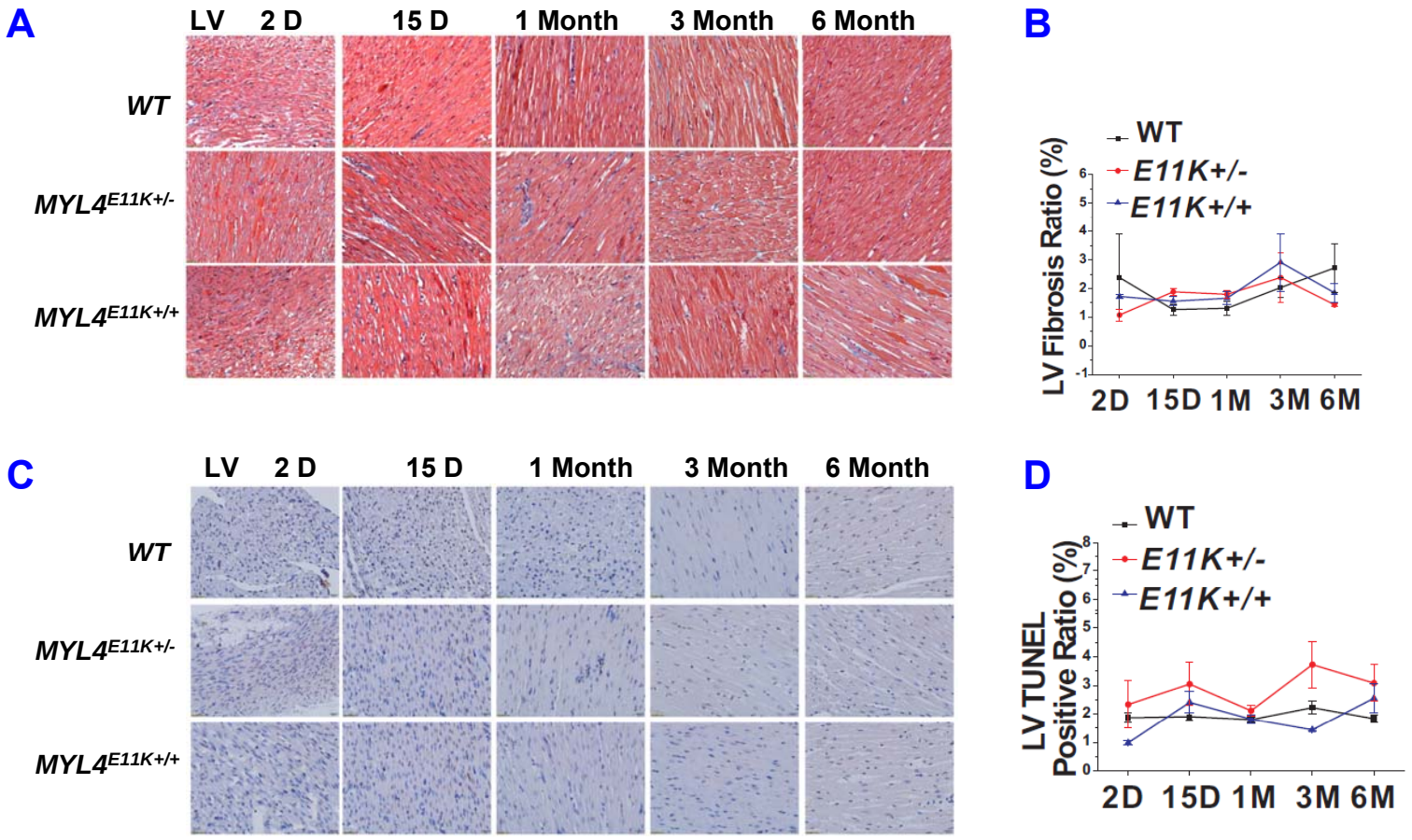

MYL4E11K does not affect ventricular fibrosis or apoptosis.
A and B: Ventricle fibrosis obtained by Masson staining averaged for 4-5 hearts per group (6-10 fields per heart for each group).
C and D: Representative images and mean data for TUNEL staining of ventricle sections from WT, *MYL4 E11K*$_{+/-}$and *MYL4 E11K*$_{+/+}$rats.

Figure S6.

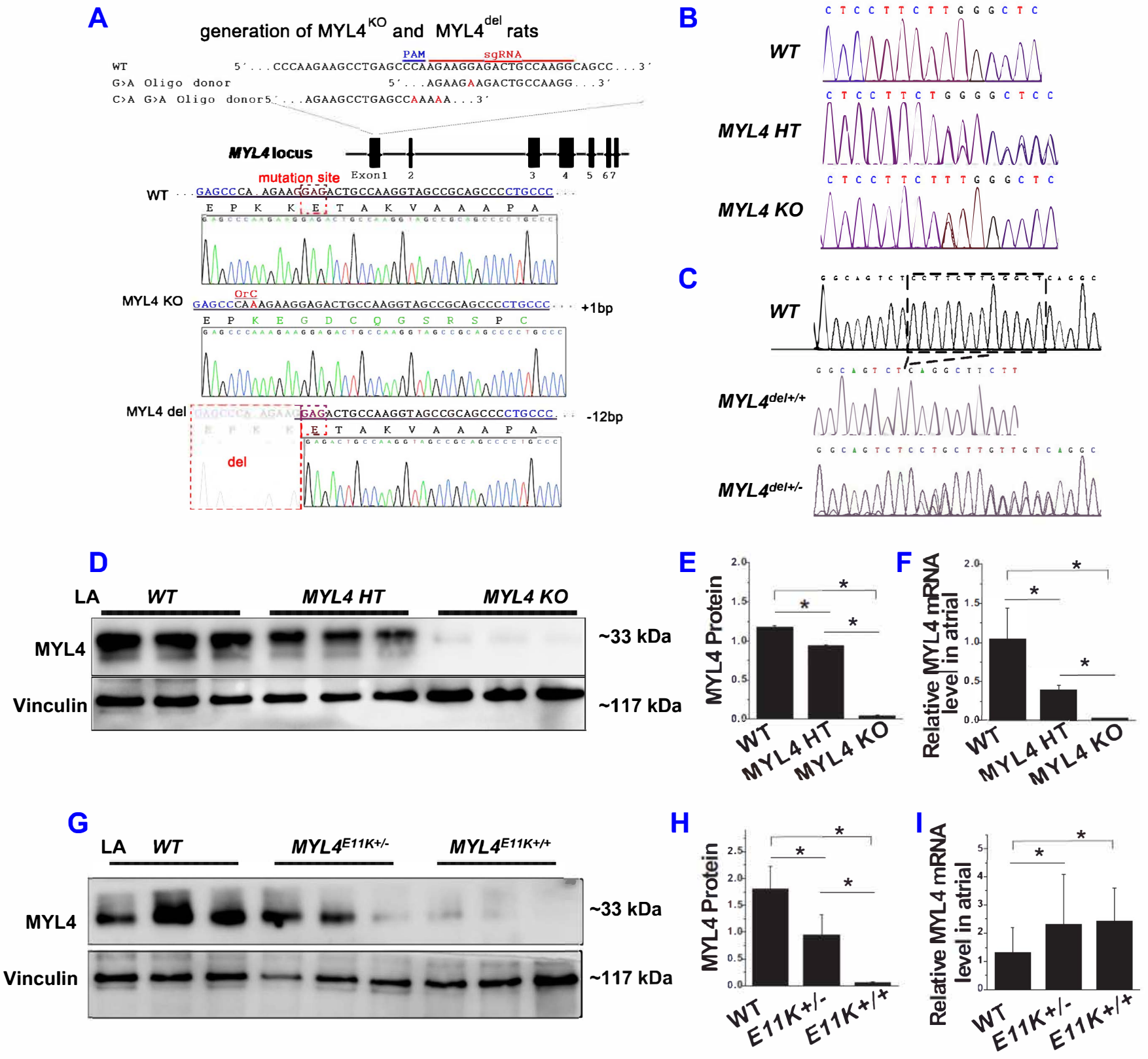

MYL4 KO and ***MYL4 del*** targeting strategies and identification.

The *MYL4 KO* and *MYL4 del* rat models were constructed using CRISPR/Cas-mediated genome editing (A). The genotypes were identified by Sanger Sequencing (B-C). *MYL4 KO* was verified by Western Blot and Real-time PCR (D-F). *MYL4 E11K* also was verified by Western Blot and Real-time PCR (G-I).

Figure S7.

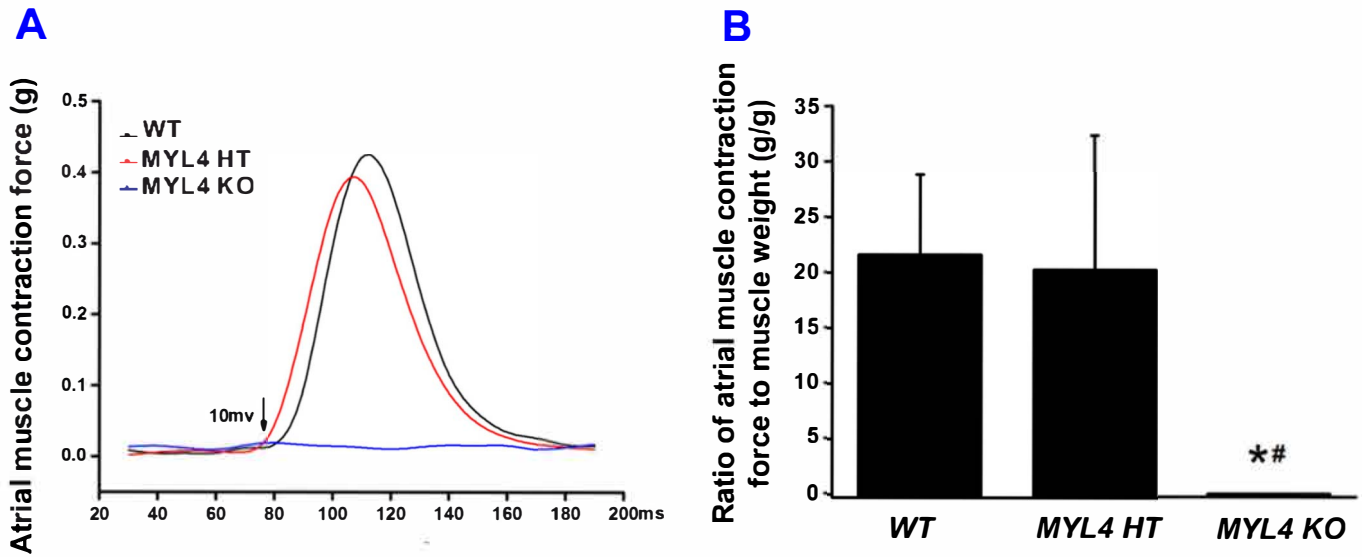

Lost atrial contractile force in *MYL4 KO* rats.

Figure S8.

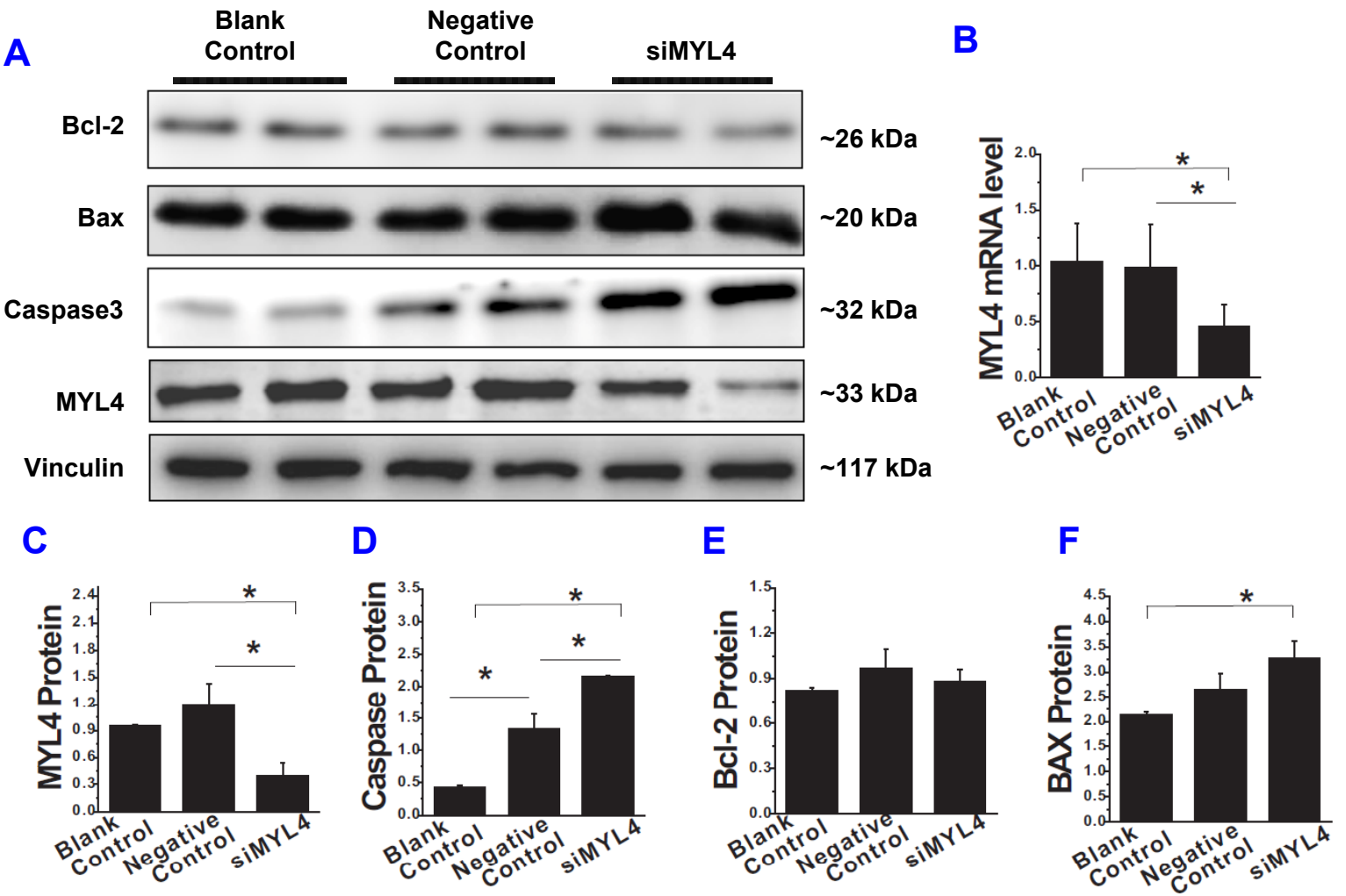

MYL4 knockdown in cultured myocytes leaded to a similar myocyte death phenotype.
MYL4 was knocked down with the use of siRNA (siMYL4: 5'-GCA CCU AUG AGG ACU UCG UTT-3'; Negative control: 5'-UUC UCC GAA CGU GUC ACG UTT-3') in cultured myocytes, caspase 3, Bax and Bcl-2 protein level were detected by WB.
Data are mean ± SEM. Protein from 3 independent samples were subjected to immunoblot for each groups. *p<0.05.

Figure S9.

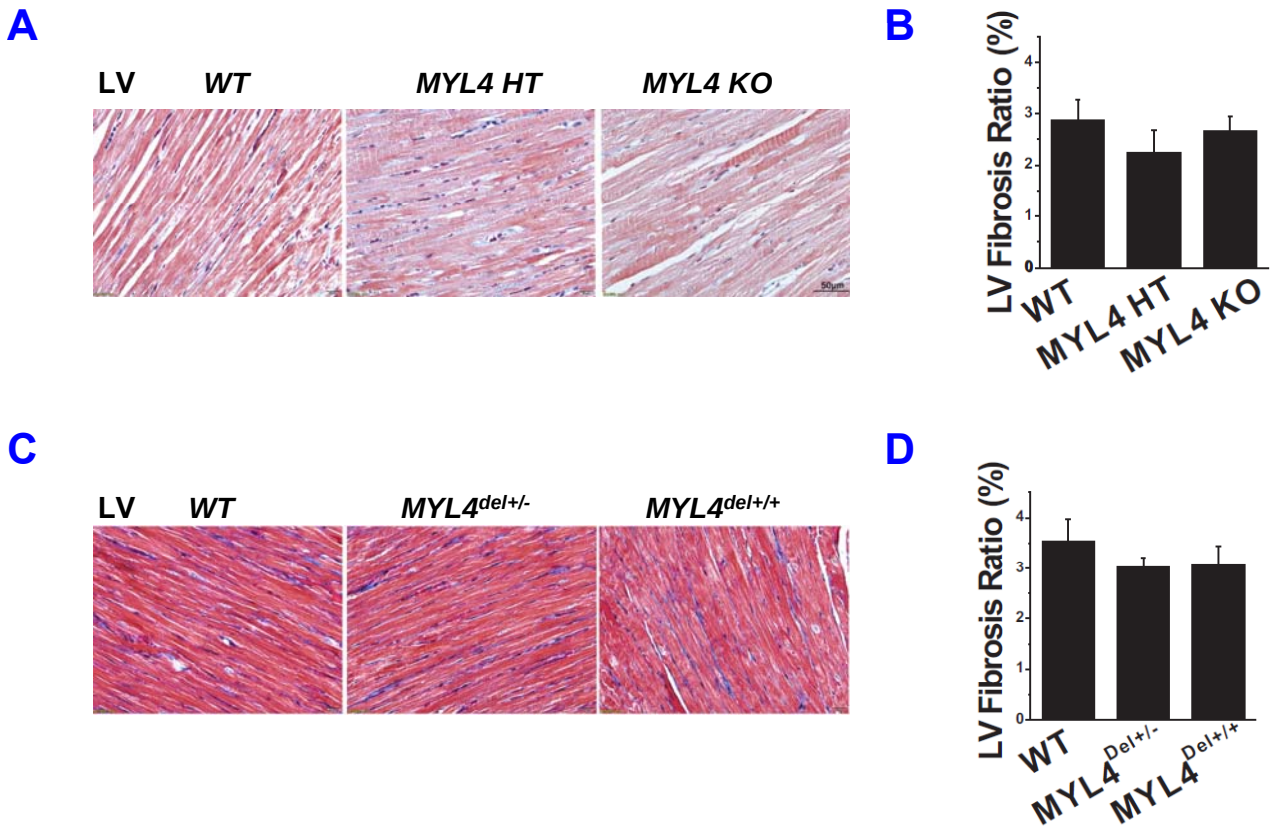

MYL4KO **or *del* mutations do not cause ventricular fibrosis.**
Ventricular fibrosis measured with Masson staining was averaged for 4-5 hearts per group (6-10 fields per heart for each group).
A-B: Ventricular fibrosis for *MYL4 KO* rats.
C-D: Ventricular fibrosis for *MYL4 del* rats.

Figure S10.

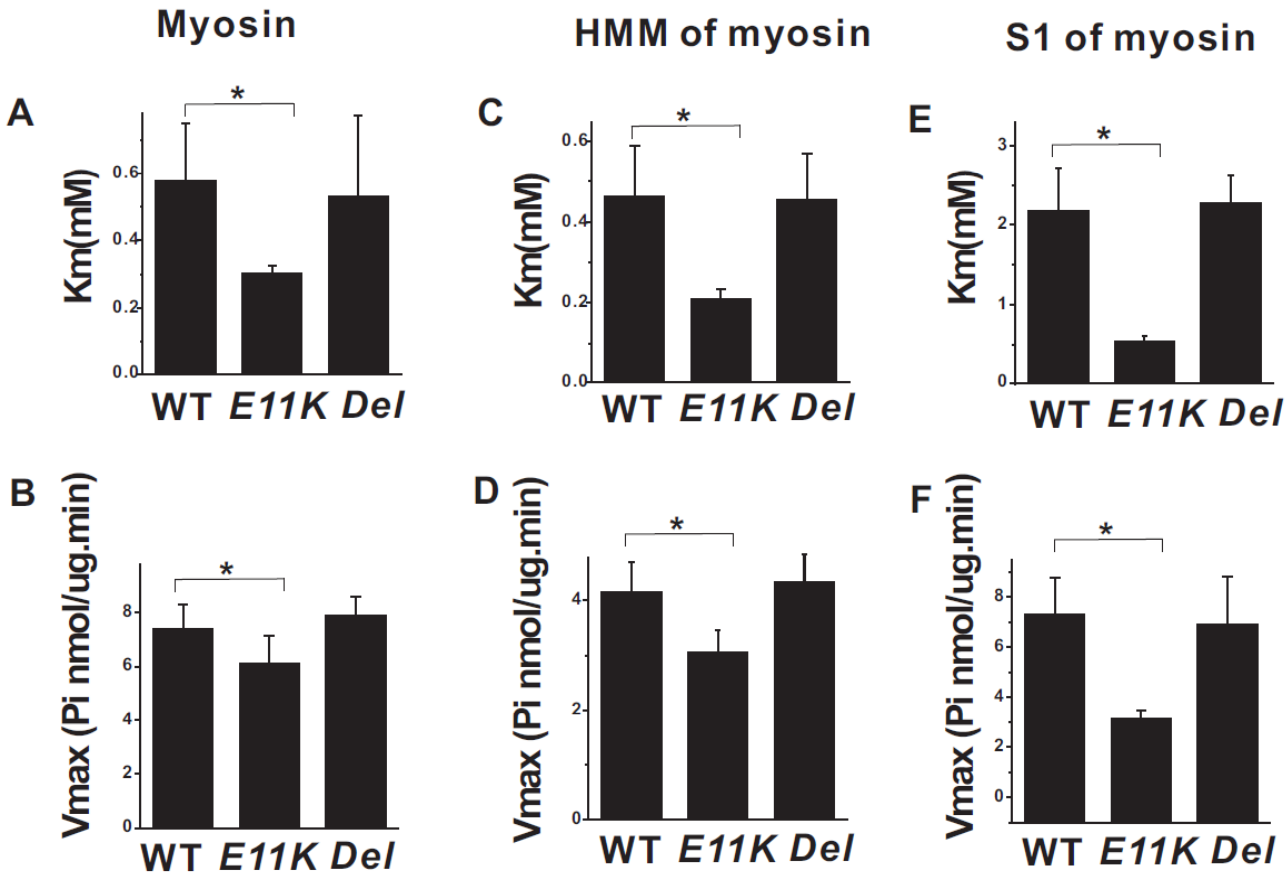

ATPase activity assays

The ATPase activities were determined based on Km and Vmax of myosin. Both Km and Vmax were significantly smaller in the presence of MYL4-E11K protein than MYL4-WT protein, but MYL4-Del protein did not affect myosin ATPase activity.

HMM: Heavy Meromyosin Protein; S1: Myosin head subfragment-1 domain. Both HMM and S1 have ATPase activity.

* $p<0.05$.